Improving and Bounding Asymptotic Approximations for Diversity Combiners in Correlated Generalized Rician Fading

by

Joshua Schlenker

B.A.Sc., The University of British Columbia, 2010

A THESIS SUBMITTED IN PARTIAL FULFILLMENT OF
THE REQUIREMENTS FOR THE DEGREE OF

MASTER OF APPLIED SCIENCE

in

The Faculty of Graduate Studies

(Electrical & Computer Engineering)

THE UNIVERSITY OF BRITISH COLUMBIA

(Vancouver)

February 2013

Abstract

Although relatively simple exact error rate expression are available for selection combining (SC) and equal gain combining (EGC) with independent fading channels, results for correlated channels are highly complex, requiring multiple levels of integration when more than two branches are involved. Not only does the complexity make numeric computation resource intensive, it obscures how channel statistics and correlation affect system performance. Asymptotic analysis has been used to derive simple error expressions valid in high signal-to-noise ratio (SNR) regimes. However, it is not clear at what SNR value the asymptotic results are an accurate approximation of the exact solution. In this thesis, we derive asymptotic results for SC, EGC, and maximal ratio combining (MRC) in correlated generalized Rician fading channels. By assuming generalized Rician fading, our results incorporate Rician, Rayleigh, and Nakagami-m fading scenarios as special cases. Furthermore, the asymptotic results for SC are expanded into an exact infinite series. Although this series grows quickly in complexity as more terms are included, truncation to even two or three terms has much greater accuracy than the first (asymptotic) term alone. Finally, we derive asymptotically tight lower

and upper bounds on the error rate for EGC. Using these bounds, we are able to show at what SNR values the asymptotic results are valid.

Table of Contents

Appendices

List of Tables

List of Figures

List of Notation

$\lvert\cdot\rvert$	Absolute value of a complex number
$I_v(\cdot)$	Modified Bessel function of the first kind with order v, $I_v(x) \triangleq \sum_{i=0}^{\infty} \frac{(x/2)^{v+2i}}{i!\Gamma(v+i+1)}$
$J_v(\cdot)$	Bessel function of the first kind with order v, $J_v(x) \triangleq \sum_{i=0}^{\infty} \frac{(-1)^i(x/2)^{v+2i}}{i!\Gamma(v+i+1)}$
$\binom{n}{k}$	Binomial coefficient, $\binom{n}{k} \triangleq \frac{n!}{k!(n-k)!}$
$\Phi_X(\cdot)$	Characteristic function of a random variable X, $\Phi_X(\omega) \triangleq \mathrm{E}\left[e^{j\omega X}\right]$
$(\cdot)^*$	Conjugate of a complex number
$F(\cdot)$	Dawson's integral, $F(x) \triangleq e^{-x^2}\int_0^x e^{t^2}dt$
$\det(\cdot)$	Determinant of a matrix
$\mathrm{E}[\cdot]$	Expectation of a random variable
$N!$	Factorial of a non-negative integer N, $N! \triangleq 1\cdot 2\cdots(N-1)\cdot N$ and $0! = 1$
$\Gamma(\cdot)$	Euler's Gamma function, $\Gamma(x) \triangleq \int_0^\infty t^{x-1}e^{-t}dt$
$\mathcal{N}(\mu,\sigma^2)$	Gaussian distribution with mean μ and variance σ^2

${}_1F_1(\cdot;\cdot;\cdot)$	Kummer confluent hypergeometric function, ${}_1F_1(a;b;x) \triangleq \sum_{i=0}^{\infty} \frac{(a)_i}{(b)_i i!} x^i$
$\Im(\cdot)$	Imaginary part of a complex number
$L_i^{(\alpha)}(\cdot)$	Generalized Laguerre polynomial with degree i and order α, $L_i^{(\alpha)}(x) \triangleq \sum_{j=0}^{i} \frac{(j+\alpha+1)_{i-j}}{(i-j)!j!}(-x)^j,\ \alpha > -1$
$Q_v(\cdot,\cdot)$	Generalized Marcum Q-function with order v, $Q_v(a,b) \triangleq \int_b^{\infty} \frac{x^v}{a^{v-1}} e^{-(x^2+a^2)/2} I_{v-1}(ax)dx$
$\mathcal{M}_X(\cdot)$	Moment generating function of a random variable X, $\mathcal{M}_X(s) \triangleq \mathrm{E}\left[e^{-sX}\right]$
$\mathbb{N}$	Set of non-negative integers $0, 1, 2, \ldots$
$(x)_n$	Pochhammer's symbol, $(x)_n \triangleq \frac{\Gamma(x+n)}{\Gamma(x)}$
$Q(\cdot)$	Gaussian Q-function, $Q(x) \triangleq \frac{1}{\sqrt{2\pi}} \int_x^{\infty} \exp\left(-t^2/2\right)dt$
$\mathbb{R}$	Set of real numbers
$\Re(\cdot)$	Real part of a complex number
$o(\cdot)$	Order of a function, a function $g(x)$ is $o(x)$ if $\lim_{x\to 0} \frac{g(x)}{x} = 0$
$(\cdot)^T$	Transpose of a vector or matrix

List of Abbreviations

AWGN	Additive White Gaussian Noise
BCFSK	Binary Coherent Frequency Shift Keying
BDPSK	Binary Differential Phase Shift Keying
BER	Bit Error Rate
BNCFSK	Binary Noncoherent Frequency Shift Keying
BPSK	Binary Phase Shift Keying
CDF	Cumulative Distribution Function
CHF	Characteristic Function
EGC	Equal Gain Combining
H-S/MRC	Hybrid Selection/Maximal Ratio Combining
i.i.d.	Independent, Identically Distributed
LOS	Line-Of-Sight
MGF	Moment Generating Function
M-PAM	M-ary Pulse Amplitude Modulation
M-PSK	M-ary Phase Shift Keying
M-QAM	M-ary Quadrature Amplitude Modulation
MRC	Maximal Ratio Combining

OFDM	Orthogonal Frequency Division Multiplexing
PDF	Probability Density Function
RF	Radio Frequency
RV	Random Variable
SC	Selection Combining
SER	Symbol Error Rate
SNR	Signal-to-Noise Ratio
w.r.t.	With Respect To

Acknowledgements

I would like to express deep gratitude to my superiors Julian Cheng and Robert Schober for their hard work and dedication to seeing me through to the end despite my doubts along the way. Without their insight and expertise I would scarcely have scratched the surface of what this project became. I also owe debts of thanks to many colleagues I have encountered in my time at UBC in Vancouver and the Okanagan, some of whom have become life long friends. Finally, I would like to thank my parents for their enduring support and my closest confidant, my girlfriend Kayla, for having the patience to stick with me through to the end.

Funding for this research was provided by the Natural Sciences and Engineering Research Council of Canada (NSERC).

Chapter 1

Introduction

1.1 Background and Motivation

In recent decades the use of wireless devices has exploded, driven mainly by the increase in consumer electronics with wireless capabilities, such as cellular phones, laptops, and GPS units. The mobile nature of these devices and the multipath propagation of the wireless signal introduces a time variation in the quality of the channel between transmitter and receiver known as fading. Without adequate mitigation of this effect, the experience to the end user would be extremely detrimental, causing dropped phone calls, inability to load webpages, etc. when a deep fade occurs. One powerful method of combating fading is known as diversity combining. Diversity combining employs multiple antennas at the receiver, with each branch experiencing different instantaneous signal-to-noise ratios (SNRs) provided the antennas are spaced sufficiently far apart. The probability that each antenna simultaneously experiences poor channel conditions decreases significantly as more antennas are added. Although many diversity combining techniques have been studied in the literature, the three most popular are selection combining (SC), equal

gain combining (EGC), and maximal ratio combining (MRC).

Although exact performance analysis of SC, EGC, and MRC has been widely studied, the results are generally complex, even for independent fading. For correlated fading with more than two branches, the results are given in terms of multiple nested infinite series or integrations even for specialized correlation matrices. This complexity obscures how performance is affected by fading parameters and the correlation among branches. In response, a number of research papers have studied the performance when SNR approaches infinity. This technique is known as asymptotic analysis. The assumption of high SNR results in a closed-form equation for performance metrics such as symbol error rate (SER) and outage probability. Although only strictly valid at infinite SNR, the exact performance can be approximated by the asymptotic results at moderate SNR levels. However, it is difficult to determine at what SNR value the approximation is valid without resorting to computationally expensive exact analytical analysis or Monte Carlo simulations, both of which are susceptible to inaccuracies at low SERs typical in the high SNR regime.

1.2 Literature Review

The performance analysis of SC, EGC, and MRC for independently faded channels has been widely studied, and SER expressions are available for a wide variety of linear modulations which only require a single level of integra-

tion regardless of the number of branches. (See [1] and the references therein.) However, correlation among branches arises when the diversity antennas are in close proximity, which occurs for devices with space constrained form factors such as mobile phones. For the general case of L diversity branches and arbitrary channel correlation, single integral forms and single infinite series exist for the error rate with MRC at the receiver [2–4]. However, error rate expressions for EGC and SC are much more complex, typically involving multi-level integration or infinite series. Expressions with a single integral or infinite series are only available when the number of branches is limited to two [5–10]. For $L > 2$, single integral or infinite series forms for the error rate are unavailable even for specialized correlation models.

Regarding the SC literature, Karagiannidis *et al.* obtained a dual infinite series representation of the error rate for a triple branch SC undergoing Nakagami-m fading with exponential branch correlation [11]. The general result for arbitrary correlation can be obtained using the joint cumulative distribution function (CDF) of three Nakagami-m random variables (RVs) obtained in [12]; however this requires an additional two infinite series. The joint CDF of L exponentially correlated Nakagami-m RVs was obtained in [13], consisting of a $L-1$ fold infinite series. The results of [13] were extended to arbitrarily correlated Nakagami-m RVs using a Green's matrix approximation of the correlation matrix [14]. Exact results for the most general case of arbitrary L and correlation matrix are available for SC but the complexity of the error rate expressions increases exponentially in L. In [15]

the authors took a characteristic function (CHF) approach independent of the fading distribution; however, the Fourier inversion requires L infinite integrals. A multivariate joint probability density function (PDF) of the general $\alpha - \mu$ distribution consisting of a single infinite sum of generalized Laguerre polynomials was derived in [16]; however, application to SC performance analysis requires an L-fold integral of the joint PDF.

The literature for EGC with $L > 2$ and correlation among the branches is limited to special correlation models and approximations. In [17], the authors found the moments at the output of an EGC combiner with Nakagami-m fading in terms of an $L-1$ fold infinite summation. The results are approximate for arbitrarily correlated branches and exact for exponential correlation. The moment generating function (MGF) can be found from the central moments via a Taylor series expansion or Padé approximation, from which the error rate follows with a single integration. A different approach was taken in [18], where the approximate PDF of a sum of correlated Nakagami-m RVs was found using moment matching. Using the joint PDF of exponentially correlated Nakagami-m RVs in [13], Sahu and Chaturvedi found the error rates for coherent BPSK [19] and noncoherent modulations [20]. However, the expressions are highly complex and involve $L-1$ fold infinite summation along with several levels of finite summation.

A novel approach was taken in [21] to find single integral representations for the CDF of the SNR at the output of a SC combiner with equally correlated Nakagami-m, Rayleigh, and Rician fading channels. The correlated

RVs are modelled using a linear combination of independent Gaussian RVs. This allowed the authors to find the error rate using two nested integrals. Using the same model as [21], Chen and Tellambura found the moments at the output of an EGC combiner for equally correlated Rayleigh, Rician, and Nakagami-m fading channels [22]. The authors then presented an approach for finding the error rate using a single infinite series of the moments. Although the joint PDF was found in single integral form, the moment expressions are L-fold summations of a Lth order Lauricella function. In [23], the model was generalized for Nakagami-m fading channels and was termed the 'generalized correlation model', which was then utilized to derive error rate and outage probability expressions for hybrid selection/maximal ratio combining (H-S/MRC). Using the generalized correlation model, Beaulieu and Hemachandra [24] derived single integral forms of the joint PDF and CDF of Rayleigh, Rician, generalized Rician, Nakagami-m, and Weibull RVs.

The results cited above all require multiple nested levels of integration to evaluate the exact SER for SC or EGC with correlated fading when $L > 2$. Asymptotic analysis allows this complexity to be circumvented by finding simple SER expressions which are valid only at asymptotically high SNR. Results for SC, EGC, and MRC are available in the literature. In [25], Li and Cheng conducted an asymptotic performance analysis for SC with Nakagami-m fading channels using the generalized correlation model. For arbitrary correlated Rician channels, the asymptotic results for SC and EGC can be found in [26]. For arbitrarily correlated Nakagami-m and Rician

channels the asymptotic technique was employed to find the SER of MRC in [27] and [28], respectively.

Although it provides insight into how correlation and fading distribution parameters affect SER, the major shortcoming of the asymptotic technique is that it can not predict at what SNR value the asymptotic solutions can adequately approximate the exact solution. Assessment of the accuracy of asymptotic solutions for a particular SNR using Monte Carlo simulations or exact analytical analysis is problematic. Monte Carlo simulation is time consuming due to the low probability of a symbol error at high SNR, and the computation of exact analytical solutions requires complex multilevel numeric integration which is also susceptible to error due to the small numerical values or oscillatory nature of the integrand over the integration region.

1.3 Thesis Outline and Contributions

The remainder of this thesis consists of five chapters. In Chapter 2, we introduce necessary background information relevant to the chapters that follow, including an overview of fading and diversity combining. Furthermore, the joint CDF and PDF of generalized Rician RVs correlated according to the generalized correlation model are derived. In Chapter 3, we find the asymptotic error rate expressions for SC, EGC, MRC. In Chapter 4, an infinite series expansion of the bit error rate (BER) of SC is derived along with the truncation error when the series is terminated at a finite number of terms.

The termination of the series to the first term is the asymptotic error rate. In Chapter 5, we develop asymptotically tight error bounds for EGC. The bounds are in the form of a single integration, comparable to the complexity of computing the exact error rate if the branches were independent. Chapters 3-5 assume generalized Rician fading with generalized correlation among branches. The results of Chapter 4 and Chapter 5 can be utilized to show at what SNR the asymptotic error rate is guaranteed to be within a specified tolerance of the exact error rate. In Chapter 6, we conclude this thesis and suggest possibilities for related future work.

Chapter 2

Fading and Diversity Combining

In this chapter, we present an overview of the challenges that fading places on reliable wireless communications and several statistical distributions commonly used to model the fading channel. We then introduce several diversity combining techniques which are used to reduce the deleterious effects of multipath fading when the transmitted signal is sent over multiple fading channels. In general, the multiple fading channels are correlated, and we introduce a method to construct generalized Rician RVs for a special correlation model known as the generalized correlation model.

2.1 Multipath Fading

When a radio frequency (RF) signal is propagated from a transmitter to receiver wirelessly it typically takes multiple paths due to scattering and reflections caused by objects in the surrounding environment include buildings, roads and cars in an urban environment, and trees and hills in a more

rural area. The number of propagation paths can be large, especially in an urban setting. Each path experiences a different attenuation and phase delay. When the signals recombine at the receiver, their constructive and destructive addition results in a phenomenon known as small-scale fading. Small-scale fading, as opposed to large-scale fading which is the result of large objects such as buildings or hills located between transmitter and receiver, is highly location specific. Even motion on the order of centimeters can cause large fluctuations in the signal strength at the receiver due to the high carrier frequencies in typical wireless communication systems. For example, if a mobile phone operates with a carries frequency of 2 GHz, with a corresponding wavelength of approximately 15 cm, even a small movement by the mobile user could cause the signal strength to transition from relatively strong to weak. In this thesis, we only consider small-scale fading, which we will simply refer to as fading. This is a common assumption in the literature.

A deterministic treatment of the wireless channel is not practical due to large number of propagation paths and random movements of the users and surrounding objects. Thus, fading is typically modelled as a random process. The fading channel is characterized by its coherence time and bandwidth. The coherence time, roughly speaking, is the length of time the fading coefficient can be considered as approximately constant. Signals with a symbol duration smaller than the coherence time will experience slow fading, where the channel conditions are constant throughout the symbol duration.

A signal with a symbol duration longer than the channel coherence time will experience fast fading, where the fading coefficient changes during symbol transmission. Coherence bandwidth is a frequency-domain description of fading channels. A transmitted symbol with a bandwidth larger than the channel coherence bandwidth will experience frequency selective fading whereas when the opposite is true, each frequency in the transmitted symbol will experience approximately identical fading resulting in frequency nonselective or flat fading. In slow, frequency nonselective fading, the channel can be described by the complex gain $he^{j\theta}$ for the duration of the transmitted symbol, where h and θ are the random fading envelope and phase respectively. We will assume slow, frequency nonselective fading in this thesis. In situations where the channel is frequency selective, it can be divided into multiple frequency nonselective channels using orthogonal frequency division multiplexing (OFDM) [30]. Though there exists a large number of statistical models for h, each tailored to specific fading environments, three widely adopted fading models are Rayleigh, Rician, and Nakagami-m.

The effect of fading on receiver performance is significant. In a constant channel gain, i.e. no fading, in the high SNR regime, a binary phase shift keying (BPSK) modulated signal has the BER

$$P_e \approx \frac{1}{2\sqrt{\pi\bar{\gamma}}} e^{-\bar{\gamma}} \tag{2.1}$$

where $\bar{\gamma}$ is the average SNR at the receiver. The identical receiver in a

Rayleigh fading channel experiences a BER at large SNR of [31]

$$P_e \approx \frac{1}{4\bar{\gamma}}. \tag{2.2}$$

In effect, the presence of fading has reduced the BER from being exponential in $\bar{\gamma}$ to only linear. At typical SNRs, fading increases the error rate by several orders of magnitude. For example, at 10 dB a constant gain channel would experience a BER of approximately 5×10^{-5}, while a Rayleigh faded channel would experience a BER of roughly 2×10^{-2}. As this is also only the average error rate, the instantaneous error rate can even be worse.

2.1.1 Rayleigh Distribution

When the complex channel gain is modelled as a zero mean Gaussian RV with independent, identically distributed (i.i.d.) real and imaginary parts, the fading envelop follows the Rayleigh distribution. This model best fits environments in which the transmitted signal is scattered and reflected multiple times before reaching the receiver without a line-of-sight (LOS) path. By a central limit theorem, the sum of all signal paths at the receiver will have a zero-mean Gaussian distribution. The Rayleigh RV X has a PDF of

$$f_X(x) = \frac{2x}{\sigma^2} e^{-\frac{x^2}{\sigma^2}} \tag{2.3}$$

where $\sigma^2/2$ is the variance of the underlying Gaussian RVs. The average power of the Rayleigh distribution is $\Omega = \mathrm{E}[X^2] = \sigma^2$. In Fig. 2.1, the Rayleigh PDF is plotted for several values of Ω. When the fading envelope is Rayleigh distributed, it can be shown that the fading power follows an exponential distribution.

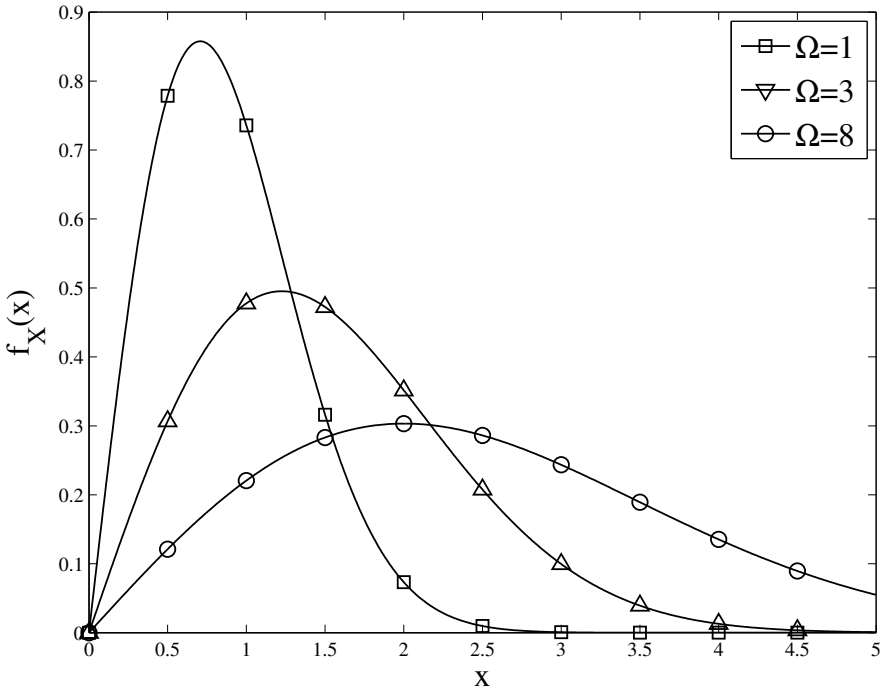

Figure 2.1: The probability density function of a Rayleigh RV with different values of Ω.

2.1.2 Rician Distribution

When a rich scattering environment similar to Rayleigh arises but with an additional LOS path between transmitter and receiver, a Rician distribution model accurately describes the fading envelope. A Rician RV can be constructed from two Gaussian RVs, $X_1 \sim \mathcal{N}\left(\mu_1, \frac{\sigma^2}{2}\right)$ and $X_2 \sim \mathcal{N}\left(\mu_2, \frac{\sigma^2}{2}\right)$, as

$$X = \sqrt{X_1^2 + X_2^2}. \tag{2.4}$$

The distribution of X is given by the Rician PDF

$$f_X(x) = \frac{2x}{\sigma^2} e^{-\frac{x^2+s^2}{\sigma^2}} I_0\left(\frac{2sx}{\sigma^2}\right) \tag{2.5}$$

where $s^2 = \mu_1^2 + \mu_2^2$ is the power due to the LOS signal. The average power is $\Omega = \mathrm{E}[X^2] = s^2 + \sigma^2$. The factor σ^2 is known as the scattering power since it is the sum power contribution of the numerous scattering and reflection paths. The ratio of LOS power to scattering power is known as the Rice factor

$$K = \frac{s^2}{\sigma^2}. \tag{2.6}$$

The Rician distribution can be rewritten in terms of K and Ω as

$$f_X(x) = \frac{2(K+1)}{\Omega} x e^{-\frac{K+1}{\Omega}x^2 - K} I_0\left(2\sqrt{\frac{K(K+1)}{\Omega}}x\right). \tag{2.7}$$

In Fig. 2.2, we have plotted the Rician PDF for several values of K. When $K = 0$, the Rician distribution specializes to the Rayleigh distribution. On the other hand, as K is increased while Ω is held constant, the probability of deep fades decreases and the Rician distribution approaches a δ pulse, which can be seen in Fig. 2.2.

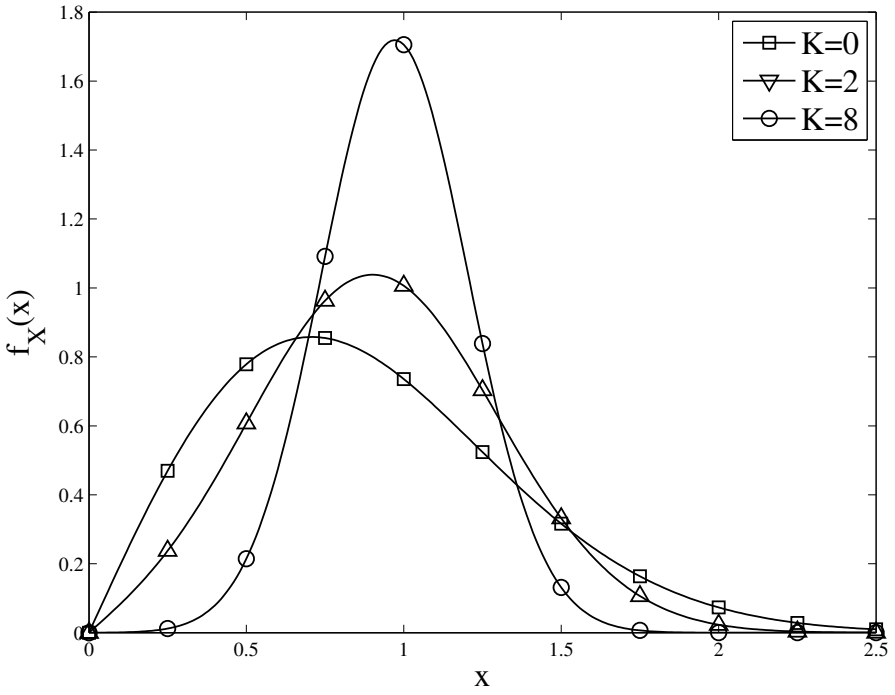

Figure 2.2: The probability density function of a Rician RV with $\Omega = 1$.

2.1.3 Nakagami-m Distribution

Another distribution with more flexibility than Rayleigh is the Nakagami-m distribution. The PDF of a Nakagami-m RV X is given by [32]

$$f_X(x) = \frac{2x^{2m-1}}{\Gamma(m)} \left(\frac{m}{\Omega}\right)^m e^{-\frac{m}{\Omega}x^2}, \quad m \geq \frac{1}{2} \tag{2.8}$$

where $\Omega = \mathrm{E}[X^2]$. The parameter m is known as the shape parameter and controls the severity of fading. When m=1, Nakagami-m reduces to the Rayleigh distribution, and $\frac{1}{2} \leq m < 1$ and $m > 1$ corresponds to more and less severe fading, respectively, than Rayleigh as shown in Fig. 2.3. The square of a Nakagami-m RV is Gamma distributed with PDF

$$f_{X^2}(x) = \frac{x^{m-1}}{\Gamma(m)} \left(\frac{m}{\Omega}\right)^m e^{-\frac{m}{\Omega}x}. \tag{2.9}$$

The Nakagami-m distribution has been shown to fit empirical data in an urban setting better than Rayleigh or Rician distributions [33]. Also a theoretical basis for modelling the outdoor mobile radio channel with the Nakagami distribution was provided by [34].

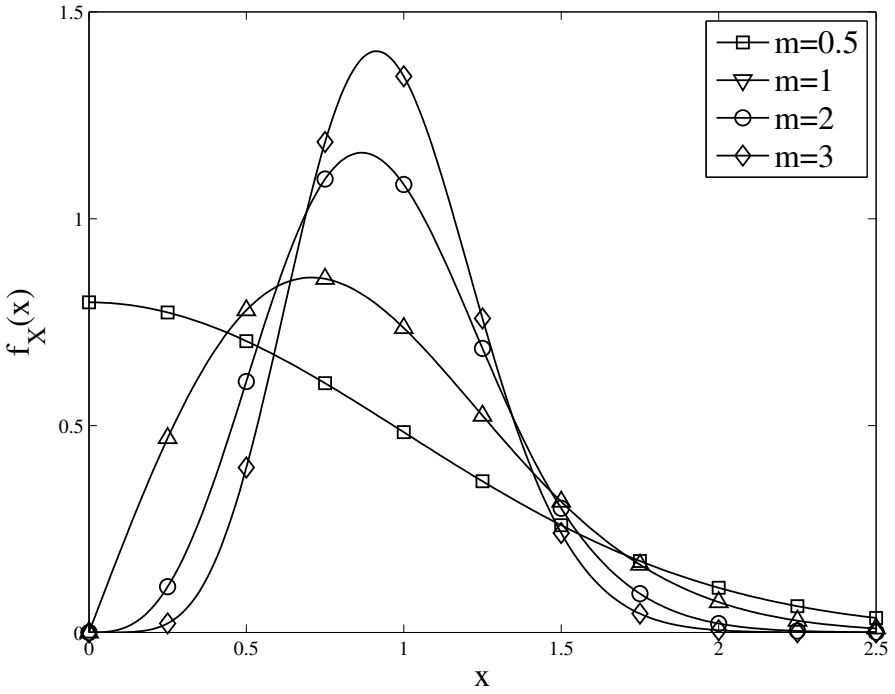

Figure 2.3: The probability density function of a Nakagami-m RV with $\Omega = 1$.

2.1.4 Generalized Rician Distribution

The Rician model can be generalized by changing (2.4) from two to an arbitrary n dimensions

$$X = \sqrt{\sum_{l=1}^{n} X_l^2} \tag{2.10}$$

where $X_l \sim \mathcal{N}(\mu_l, \sigma^2/2), l = 1, 2, \ldots, n$ are independent. The generalized Rician PDF is given by

$$f_X(x) = \frac{2x^{\frac{n}{2}}}{\sigma^2 s^{\frac{n}{2}-1}} e^{-\frac{x^2+s^2}{\sigma^2}} I_{\frac{n}{2}-1}\left(\frac{2sx}{\sigma^2}\right) \tag{2.11}$$

where $s^2 = \sum_{l=1}^{n} \mu_l^2$ and $\Omega = E[X^2] = s^2 + \frac{n}{2}\sigma^2$.

Although the generalized Rician model is not typically used to model fading due to a lack of theoretical or empirical justification, it does incorporate the three previous models to some extent. Obviously with $n = 2$ it specializes to the Rician distribution, and with $n = 2$, $s = 0$ we obtain the Rayleigh distribution. Although not as obvious, the generalized Rician distribution also specializes to the Nakagami-m distribution. Consider X^2 with $s = 0$, which is the sum of n independent squared Gaussian RVs with identical variances and zero means, hence X^2 follows the chi-square distribution and has a PDF of

$$f(x) = \frac{2x^{n-1}}{\Gamma\left(\frac{n}{2}\right)} \left(\frac{n}{2\Omega}\right)^{\frac{n}{2}} e^{-\frac{x}{\sigma^2}} \tag{2.12}$$

which matches (2.9) when $m = \frac{n}{2}$. Thus, when m is a integer or half integer the Nakagami-m distribution is a special case of generalized Rician distribution. In this thesis, we will assume generalized Rician fading since it includes the other three fading models as special cases.

2.2 Diversity Combining

A common method for mitigating fading is to employ diversity at the receiver. Multiple copies of the transmitted signal are made available to the receiver, each experiencing different fading channels. The probability that all fading channels are in deep fade simultaneously decreases rapidly as diversity is increased. Receive diversity can be achieved by transmitting the same symbol over multiple frequencies or time slots. However, this requires additional bandwidth. To circumvent this problem, the receiver can employ multiple antennas, each receiving the transmitted signal over different fading channels. In general, the channels are correlated due to space constraints in small form factors, such as mobile phones, which requires antennas to be in close proximity. Branches in a system employing time or frequency diversity will be correlated if duplicate transmissions occur within the coherence time or coherence bandwidth respectively.

There are several methods to combine the received signals, each with a different performance-complexity trade off. Suppose that the receiver has L branches of diversity available, and the transmitted symbol with energy E_S is subject to a fading channel with complex channel gain $h_k e^{j\theta_k}$ and additive white Gaussian noise (AWGN) with power spectral density N_0 on the kth branch. The instantaneous SNR on branch k is then $\gamma_k = h_k^2 \frac{E_S}{N_0}$. A linear combiner multiplies the signal on the kth branch by a complex weight w_k, then sums the result. The instantaneous SNR at the output of a general

linear combiner is then

$$\gamma_c = \frac{\left|\sum_{k=1}^{L} w_k h_k e^{j\theta_k}\right|^2}{\sum_{k=1}^{L} |w_k|^2} \frac{E_S}{N_0}. \tag{2.13}$$

The simplest combining technique would be to only consider the branch with the largest SNR and perform signal detection on this branch exclusively. This technique is known as SC. For SC, $w_i = 1$ and $\{w_k = 0,\ k = 1, 2, \ldots, L,\ k \neq i\}$ where $i = \arg\max_{k=1,2,\ldots,L} \gamma_k$. SC has an instantaneous SNR at the combiner output of

$$\gamma_{SC} = \max_{k=1,2,\ldots,L} \gamma_k. \tag{2.14}$$

Beyond its implementation simplicity, SC is also advantageous for noncoherent modulations since it does not require knowledge of the channel phases.

Although all the other branches may have lower SNRs, they still contain valuable information about the transmitted signal. A more complex combining technique that utilizes all available branches is known as EGC. EGC uses the weight $w_k = e^{-j\theta_k}$, phase aligning each branch before summation. This technique requires phase knowledge for each branch and is suitable only for coherent modulations. EGC has an instantaneous SNR of

$$\gamma_{EGC} = \frac{\left(\sum_{k=1}^{L} \sqrt{\gamma_k}\right)^2}{L}. \tag{2.15}$$

Although performance of EGC is better in most cases than SC, this may not be true in severe fading [35] or exponentially decaying average branch SNRs [36].

With EGC, we treat each branch identically regardless of the individual SNRs of each branch. A more sophisticated method is to weigh the contribution of each branch according to the severity of the fading by recognizing that branches with high SNR are more trustworthy than those with lower SNR. This combining method is known as MRC, which has the weight $w_k = h_k e^{-j\theta_k}$. MRC has an instantaneous SNR at the output of the combiner of

$$\gamma_{MRC} = \sum_{k=1}^{L} \gamma_k. \tag{2.16}$$

Applying the Cauchy-Swartz inequality to (2.13), one can prove that MRC is the optimal linear combining scheme in terms of maximizing the combiner output SNR. Although MRC is optimal, it requires knowledge of the fading envelope and phase, thus analysis of the simpler EGC and SC is of practical interest.

2.3 Generalized Correlation Model

In general, the fading channels of a diversity combiner are correlated, thus we require the joint statistics of the channel to analyze combiner performance. In this section, we present the method of Beaulieu and Hemachandra for obtaining single integral representations of the multivariate joint PDF and

CDF of correlated generalized Rician RVs [24]. Consider the following[1]

$$X_{kl} = \sigma_k \left(\sqrt{1-\lambda_k^2} U_{kl} + \lambda_k U_{0l} \right), \; k = 1, 2, \ldots, L, \; l = 1, 2, \ldots, n \tag{2.17}$$

where $-1 < \lambda_k < 1$, $\{U_{kl} \sim \mathcal{N}(0, \frac{1}{2}), k = 1, 2, \ldots, L, l = 1, 2, \ldots, n\}$, and $\{U_{0l} \sim \mathcal{N}\left(m_l, \frac{1}{2}\right), l = 1, 2, \ldots, n\}$, U_{kl} and U_{ij} are independent for $k \neq i$ or $l \neq j$. Each X_{kl} is the sum of independent Gaussian RVs and hence a Gaussian RV itself with $X_{kl} \sim \mathcal{N}\left(\sigma_k \lambda_k m_l, \frac{\sigma_k^2}{2}\right)$. For a given l, U_{0l} is common to X_{kl} for $k = 1, 2, \ldots, L$, it then follows that the X_{kl}'s are correlated RVs. Define the correlation coefficient between two RVs X and Y as

$$\rho_{XY} \triangleq \frac{\mathrm{E}[XY] - \mathrm{E}[X]\,\mathrm{E}[Y]}{\sqrt{\mathrm{Var}[X]\mathrm{Var}[Y]}} \tag{2.18}$$

where $\mathrm{Var}[X]$ is the variance of RV X. The correlation coefficient between X_{kl} and X_{ij} is given by

$$\rho_{X_{kl}X_{ij}} = \begin{cases} 1 & k = i, \; l = j \\ \lambda_k \lambda_i & k \neq i, \; l = j \\ 0 & l \neq j \end{cases}. \tag{2.19}$$

[1]We have removed the imaginary part of [24, Eq. (11)] to match the conventional form of the generalized Rician model given in [31].

Since for a given k, the X_{kl} are a set of independent Gaussian RVs with identical variance σ_k and non-zero means, $G_k = \sum_{l=1}^{n} X_{kl}^2$ and $R_k = \sqrt{G_k}$, $k = 1, 2, \ldots L$, are a noncentral χ^2 and generalized Rician RV, respectively. It is shown in Appendix A that the correlation between G_i and G_k is

$$\rho_{G_k G_i} = \rho_{R_k^2 R_i^2} = \frac{\lambda_k^2 \lambda_i^2 (\frac{n}{2} + 2S^2)}{\sqrt{\frac{n}{2} + 2\lambda_k^2 S^2}\sqrt{\frac{n}{2} + 2\lambda_i^2 S^2}}, \quad k \neq i \tag{2.20}$$

where $S^2 = \sum_{l=1}^{n} m_l^2$. For Nakagami-$m$ fading, (2.20) reduces to

$$\rho_{G_k G_i} = \rho_{R_k^2 R_i^2} = \lambda_k^2 \lambda_i^2, \quad k \neq i. \tag{2.21}$$

To find the joint PDF of $\mathbf{R} = [R_1, R_2, \ldots, R_L]$, we remove the dependence by conditioning X_{kl} on U_{0l}, which is a Gaussian RV with $\mathrm{E}[X_{kl}|U_{0l}] = \sigma_k \lambda_k U_{0l}$ and $\Omega_k = \mathrm{Var}[X_{kl}|U_{0l}] = \frac{\sigma_k^2(1-\lambda_k^2)}{2}$. It follows then that G_k conditioned on $U_{0l},\ l = 1, 2, \ldots, n$ is noncentral χ^2 distributed with PDF

$$f_{G_k|T}(g_k) = \frac{1}{2\Omega_k^2} \left(\frac{g_k}{\sigma_k^2 \lambda_k^2 T} \right)^{\frac{n-2}{4}} e^{-\frac{x + \lambda_k^2 \sigma_k^2 T}{2\Omega_k^2}} I_{\frac{n}{2}-1} \left(\frac{\sqrt{g_k \sigma_k^2 \lambda_k^2 T}}{\Omega_k^2} \right) \tag{2.22}$$

where $T = \sum_{l=1}^{n} U_{0l}^2$, and we have used the fact that conditioning on $U_{0l},\ l = 1, 2, \ldots, n$ is identical to conditioning on T. T is a noncentral χ^2 RV with PDF

$$f_T(t) = \left(\frac{t}{S^2} \right)^{\frac{n-2}{4}} e^{-(t+S^2)} I_{\frac{n}{2}-1} \left(2S\sqrt{t} \right). \tag{2.23}$$

Since G_k's conditioned on T are independent, the joint PDF of $\mathbf{G} = [G_1, G_2, \ldots, G_L]$

conditioned on T is then

$$f_{\mathbf{G}|T}(g_1, g_2, \ldots, g_L) = \prod_{k=1}^{L} \frac{1}{2\Omega_k^2} \left(\frac{g_k}{\sigma_k^2 \lambda_k^2 T} \right)^{\frac{n-2}{4}} e^{-\frac{g_k + \lambda_k^2 \sigma_k^2 T}{2\Omega_k^2}} I_{\frac{n}{2}-1} \left(\frac{\sqrt{g_k \sigma_k^2 \lambda_k^2 T}}{\Omega_k^2} \right). \tag{2.24}$$

We obtain the joint PDF of $\mathbf{G}$ by taking the expectation of (2.24) with respect to (w.r.t.) the PDF of T

$$\begin{aligned} f_{\mathbf{G}}(g_1, g_2, \ldots, g_L) &= \int_0^\infty \left(\frac{t}{S^2} \right)^{\frac{n-2}{4}} e^{-(t+S^2)} I_{\frac{n}{2}-1} \left(2S\sqrt{t} \right) \\ &\times \prod_{k=1}^{L} \frac{1}{2\Omega_k^2} \left(\frac{g_k}{\sigma_k^2 \lambda_k^2 t} \right)^{\frac{n-2}{4}} \exp\left(-\frac{g_k + \lambda_k^2 \sigma_k^2 t}{2\Omega_k^2} \right) I_{\frac{n}{2}-1} \left(\frac{\sqrt{g_k \sigma_k^2 \lambda_k^2 t}}{\Omega_k^2} \right) dt. \end{aligned} \tag{2.25}$$

By definition, the joint CDF of $\mathbf{G}$ is

$$\begin{aligned} &F_{\mathbf{G}}(g_1, g_2, \ldots, g_L) \\ &\quad = \int_0^{g_1} \int_0^{g_2} \cdots \int_0^{g_L} f_{\mathbf{G}}(x_1, x_2, \ldots, x_L) dx_1 dx_2 \cdots dx_L \\ &\quad = \int_0^\infty \left(\frac{t}{S^2} \right)^{\frac{n-2}{4}} e^{-(t+S^2)} I_{\frac{n}{2}-1} \left(2S\sqrt{t} \right) \prod_{k=1}^{L} \left[1 - Q_{\frac{n}{2}} \left(\sqrt{\frac{2\lambda_k^2 t}{1-\lambda_k^2}}, \frac{\sqrt{g_k}}{\Omega_k} \right) \right] dt \end{aligned} \tag{2.26}$$

where we have used the property $Q_v(a, 0) = 1$. We can now obtain the joint

CDF of $\mathbf{R}$ from (2.26) as follows

$$\begin{aligned}
&F_{\mathbf{R}}(r_1,r_2,\ldots,r_L)\\
&\quad=\Pr\left[r_1\le\sqrt{G_1},r_2\le\sqrt{G_2},r_L\le\sqrt{G_L}\right]\\
&\quad=F_{\mathbf{G}}(r_1^2,r_2^2,\ldots,r_L^2)\\
&\quad=\int_0^\infty\left(\frac{t}{S^2}\right)^{\frac{n-2}{4}}e^{-(t+S^2)}I_{\frac{n}{2}-1}\left(2S\sqrt{t}\right)\prod_{k=1}^{L}\left[1-Q_{\frac{n}{2}}\left(\sqrt{\frac{2\lambda_k^2t}{1-\lambda_k^2}},\frac{r_k}{\Omega_k}\right)\right]dt.
\end{aligned}\tag{2.27}$$

Taking the partial differentiation of (2.27) w.r.t. $r_1,r_2,\ldots,r_L$, we obtain the joint PDF of $\mathbf{R}$ as

$$\begin{aligned}
f_{\mathbf{R}}(r_1,r_2,\ldots,r_L)&=\frac{\exp\left(-S^2\right)}{S^{\frac{n}{2}-1}}\int_0^\infty t^{\frac{n-2}{4}}\exp\left(-t\right)I_{\frac{n}{2}-1}(2S\sqrt{t})\\
&\times\prod_{k=1}^{L}\frac{r_k^{\frac{n}{2}}}{\left(\lambda_k^2\sigma_k^2t\right)^{\frac{n-2}{4}}\Omega_k^2}\exp\left\{-\frac{r_k^2+\lambda_k^2\sigma_k^2t}{2\Omega_k^2}\right\}I_{\frac{n}{2}-1}\left(\frac{r_k\sqrt{\sigma_k^2\lambda_k^2t}}{\Omega_k^2}\right)dt.
\end{aligned}\tag{2.28}$$

Although [24] justifies the relevance of the generalized correlation model by pointing out the lack of simple PDF and CDF expressions for commonly used fading models with $L>2$, it does not discuss the limitations of the model. Let us examine the marginal PDF of R_k, which can be found by setting $r_i=\infty$ for $i=1,2,\ldots,L,\ i\neq k$ in (2.27), then differentiating w.r.t.

to r_k to obtain

$$f_{R_k}(r_k) = \frac{2r_k^{\frac{n}{2}}}{(\lambda_k \sigma_k S)^{\frac{n}{2}-1}\sigma_k^2} \exp\left(-\lambda_k^2 S^2 - \frac{r_k^2}{\sigma_k^2}\right) I_{\frac{n}{2}-1}\left(\frac{2\lambda_k S r_k}{\sigma_k}\right) \tag{2.29}$$

where we have also used the integral identity [37, Eq. (3.25.17.1)]. Comparing (2.29) to the generalized Rician PDF (2.11), we see that $s_k^2 = \lambda_k^2 \sigma_k^2 S^2$ in the generalized correlation model. Since the parameter S is identical in the marginal PDF of each R_k, $k = 1, 2, \ldots, L$, s_i cannot be chosen independently of s_k for $i \neq k$. For Rician fading, this translates to a dependence among the Rice factors. Of course, this limitation does not apply to the Rayleigh and Nakagami-m special cases since $s_k = 0$. The second limitation is that the power correlation coefficients of $\mathbf{R}$ (2.20) cannot be arbitrarily chosen for $L > 3$. There are $(L^2 - L)/2$ correlation coefficients, but only L number of λ coefficients. When $L > 3$, $(L^2 - L)/2 > L$ and there are not enough degrees of freedom available to arbitrarily choose each correlation coefficient. The generalized correlation model does however include the special case of equal correlation when $\lambda_k = \lambda$, $k = 1, 2, \ldots L$. Despite the limitations we have outlined here, we will adopt the generalized correlation model for this thesis in the absence of a tractable analytical model for arbitrary correlation.

Chapter 3

Asymptotic Performance Analysis of Combining Methods in Generalized Rician Fading

In this chapter, we derive the asymptotic error rates of SC, EGC, and MRC for coherent and noncoherent modulations in correlated generalized Rician fading channels. Although using our results, asymptotic error rates can be found for all combinations of signal modulations and combining schemes we consider, some of combinations are not useful in practice, e.g. asymptotic error rates of noncoherent modulations with EGC and MRC combiners.

As mentioned in Chapter 1, some results derived here are not original, as asymptotic error rate expressions for Rician and Nakagami-m fading with generalized correlation are a special case of those in [26–28]. The case of Nakagami-m fading with SC is also identical to the results in [25]. However, the asymptotic SC results are expanded into an exact infinite series in Chapter 4 with an upper bound on the truncation error. In addition, asymptotically tight bounds on the error rate under EGC are derived in Chapter 5.

The results of Chapters 4 and 5 can guarantee the minimum SNR at which the asymptotic error rates given here are within a tolerance of the exact error rate. The results for MRC are derived here for completeness and for comparison to SC and EGC.

3.1 System Model

Consider an L-branch diversity combiner where the transmitted signal is impaired by slow, frequency nonselective fading and AWGN on each branch. The instantaneous SNR on the kth branch is $\gamma_k = R_k^2$, where R_k is a generalized Rician RV. We assume correlation among branches fits the generalized correlation model discussed in Chapter 2, then the average SNR on the kth branch is $\overline{\gamma}_k = \mathrm{E}[\gamma_k] = \sigma_k^2 \left(\frac{n}{2} + \lambda_k^2 S^2\right)$, and power correlation between the kth and ith branch is

$$\rho_{\gamma_k \gamma_i} = \frac{\lambda_k^2 \lambda_i^2 (\frac{n}{2} + 2S^2)}{\sqrt{\frac{n}{2} + 2\lambda_k^2 S^2}\sqrt{\frac{n}{2} + 2\lambda_i^2 S^2}}, \quad k \neq i. \tag{3.1}$$

3.2 Asymptotic Analysis

Let us assume a generic receiver where γ is the instantaneous SNR at the demodulator with average SNR $\overline{\gamma} = \mathrm{E}[\gamma]$ and PDF $f_\gamma(\gamma)$. If the conditional SER for a constant (non fading) channel is $P_{e|\gamma}$, then the SER for a fading

channel is given by

$$P_e = \int_0^\infty P_{e|\gamma} f_\gamma(\gamma) d\gamma. \tag{3.2}$$

It turns out that when the average SNR approaches infinity, the error probability is solely determined by the shape of the $f_\gamma(\gamma)$ at the origin [27]. This can be intuitively explained as follows. The conditional error rate decreases exponentially in SNR due to the nature of Gaussian noise, thus even for moderate $\bar{\gamma}$, P_e is mostly determined by the probability that γ is small since $P_{e|\gamma}$ will be several orders of magnitude greater at $\gamma = 0$ than at $\gamma = \bar{\gamma}$. Let the first-order approximation of $f_\gamma(\gamma)$ at the origin be given by

$$f_\gamma(\gamma) = a\gamma^t + o(\gamma^t). \tag{3.3}$$

Using (3.3) in conjunction with (3.2) we can produce an approximation of P_e. As $\bar{\gamma} \to \infty$, P_e is increasingly dominated by the probability that γ is near zero, and the approximation approaches the exact solution.

At high SNR, many coherent modulations have a conditional error probability in the form of $pQ(\sqrt{q\gamma})$ including BPSK, M-ary pulse amplitude modulation (M-PAM), M-ary phase shift keying (M-PSK), and M-ary quadrature amplitude modulation (M-QAM) [31]. The parameters p and q for these modulations are listed in Table 3.1. The asymptotic SER with conditional error probability $pQ(\sqrt{q\gamma})$ and the first-order approximation of the

SNR PDF (3.3) is given by [27]

$$P_{e,c}^{\infty} = \frac{2^t a \Gamma(t+\frac{3}{2}) p}{\sqrt{\pi}(t+1) q^{t+1}}. \tag{3.4}$$

Table 3.1: Parameters p and q for various coherent modulations

Modulation	p	q
BPSK	1	2
M-PAM	$2\left(1-\frac{1}{M}\right)$	$\frac{6}{M^2-1}$
M-PSK ($M \geq 4$)	2	$2\sin^2\frac{\pi}{M}$
M-QAM	$4\left(1-\frac{1}{\sqrt{M}}\right)$	$\frac{3}{M-1}$

On the other hand, the noncoherent modulations binary differential phase shift keying (BDPSK) and binary noncoherent frequency shift keying (BNCFSK) have a conditional error probability of the form $\frac{1}{2}\exp(-q\gamma)$ with $q = 1$ for BDPSK, and $q = 1/2$ for BNCFSK. When the conditional error rate is given by $\frac{1}{2}\exp(-q\gamma)$ and first-order approximation of the SNR PDF is given by (3.3), the asymptotic error rate becomes [25]

$$P_{e,nc}^{\infty} = \frac{a\Gamma(t+1)}{2q^{t+1}}. \tag{3.5}$$

Since we are considering diversity combiners, γ is the output SNR of the diversity combiner, which we denote γ_{XX} where $XX = SC$, EGC, or MRC depending on the combiner under consideration. It is straight forward to determine the asymptotic SER of many coherent and noncoherent modulations by obtaining the parameters a and t from (3.3) provided that the PDF

at the output of the combiner, $f_{\gamma_{XX}}(\gamma)$, is available. While this approach is feasible for SC, it is difficult to directly determine the PDF of the sum of RVs directly, as is the case with MRC and EGC. In these cases, a Laplace transform approach is often employed. For this approach, we require the MGF of γ, defined as $\mathcal{M}_\gamma(s) = \mathrm{E}\left[e^{-s\gamma}\right]$, to be

$$\mathcal{M}_\gamma(s) = \frac{a\Gamma(t+1)}{s^{t+1}} + o\left(\frac{1}{s^{t+1}}\right) \tag{3.6}$$

as $s \to \infty$. Alternatively, we can also find a, and t from the MGF of the equivalent channel at the output of the combiner, $h = \sqrt{\gamma}$. The MGF of h when $s \to \infty$ is

$$M_h(s) = \frac{2a\Gamma(2t+2)}{s^{2t+2}} + o\left(\frac{1}{s^{2t+2}}\right). \tag{3.7}$$

3.3 First Order Joint Distributions

In order to determine the first-order approximation of γ at the origin we first find the joint PDF and the joint CDF of $\mathbf{R} = [R_1, R_2, \ldots, R_L]$ near the origin. From a Taylor series expansion of the exponential function, $\lim_{x\to 0} \exp(x) = 1 + o(1)$ and from the series expansion of the modified Bessel function of the first kind [39, Eq. (9.6.10)], $\lim_{x\to 0} I_v(x) = \frac{1}{\Gamma(v+1)}\left(\frac{1}{2}x\right)^v + o(x^{v+1})$. Substituting these asymptotic expression into the joint PDF of $\mathbf{R}$ (2.28) we find

$$f_{\mathbf{R}}(r_1, \ldots, r_L) = \frac{2^L e^{-\frac{\Lambda}{\Lambda+1}S^2}}{\Gamma^L\left(\frac{n}{2}\right)\det^{\frac{n}{2}}(\mathbf{M})\left(\prod_{k=1}^{L}\sigma_k^2\right)^{\frac{n}{2}}} \prod_{k=1}^{L}(r_k^{n-1} + o(r_k^{n-1})) \tag{3.8}$$

where $\Lambda = \sum_{k=1}^{L} \frac{\lambda_k^2}{1-\lambda_k^2}$. In obtaining (3.8), we have used an integral identity [40, Eq. (6.643.2)] and performed algebraic simplifications using [40, Eq. (9.220.2)] and [39, Eq. (13.6.12)]. We have also introduced the correlation matrix $\mathbf{M}$

$$\mathbf{M} = \begin{pmatrix} 1 & \lambda_1\lambda_2 & \cdots & \lambda_1\lambda_L \\ \lambda_1\lambda_2 & 1 & \cdots & \vdots \\ \vdots & \vdots & \ddots & \lambda_{L-1}\lambda_L \\ \lambda_1\lambda_L & \cdots & \lambda_{L-1}\lambda_L & 1 \end{pmatrix} \tag{3.9}$$

where $\det(\mathbf{M}) = \left[1 + \sum_{k=1}^{L} \frac{\lambda_k^2}{1-\lambda_k^2}\right] \prod_{k=1}^{L}(1-\lambda_k^2)$. This result can be found by expressing $\mathbf{M}$ as a rank 1 update matrix and using a matrix determinant lemma [25]. The off diagonal elements of $\mathbf{M}$ are the correlation coefficients of the underlying Gaussian RVs in $\mathbf{R}$ which were given in (2.19). The CDF of $\mathbf{R}$ can be found by integrating (3.8) over $r_1, r_2, \ldots, r_L$, resulting in

$$F_{\mathbf{R}}(r_1, \ldots, r_L) = \frac{e^{-\frac{\Lambda}{\Lambda+1}S^2}}{\Gamma^L\left(\frac{n}{2}+1\right)\det^{\frac{n}{2}}(\mathbf{M})\left(\prod_{k=1}^{L}\sigma_k^2\right)^{\frac{n}{2}}} \prod_{k=1}^{L}(r_k^n + o(r_k^n)). \tag{3.10}$$

3.4 Combiner Asymptotics

3.4.1 SC

From (2.14), the CDF of γ_{SC} can be related to $F_{\mathbf{R}}(r_1, \ldots, r_L)$ via

$$\begin{aligned} F_{\gamma_{SC}}(\gamma) &= \Pr[\gamma_1 \leq \gamma, \gamma_2 \leq \gamma, \ldots, \gamma_L \leq \gamma] \\ &= \Pr[R_1 \leq \sqrt{\gamma}, R_2 \leq \sqrt{\gamma}, \ldots, R_L \leq \sqrt{\gamma}] \\ &= F_{\mathbf{R}}\left(\sqrt{\gamma}, \ldots, \sqrt{\gamma}\right). \end{aligned} \tag{3.11}$$

Substituting (3.10) into (3.11) and differentiating w.r.t. γ we obtain the PDF of γ_{SC} as $\gamma \to 0$ as

$$f_{\gamma_{SC}}(\gamma) = \frac{nLe^{-\frac{\Lambda}{\Lambda+1}S^2}\gamma^{\frac{nL}{2}-1}}{2\Gamma^L\left(\frac{n}{2}+1\right)\det^{\frac{n}{2}}(\mathbf{M})\left(\prod_{k=1}^{L}\sigma_k^2\right)^{\frac{n}{2}}} + o(\gamma^{\frac{nL}{2}-1}). \tag{3.12}$$

Extracting the parameters a and t from (3.12), we have

$$a_{SC} = \frac{nLe^{-\frac{\Lambda}{\Lambda+1}S^2}}{2\Gamma^L\left(\frac{n}{2}+1\right)\det^{\frac{n}{2}}(\mathbf{M})\left(\prod_{k=1}^{L}\sigma_k^2\right)^{\frac{n}{2}}} \tag{3.13}$$

and

$$t_{SC} = \frac{nL}{2} - 1. \tag{3.14}$$

3.4.2 EGC

For EGC, we consider the equivalent channel gain at the output of the EGC

$$\begin{aligned} h_{EGC} &\triangleq \sqrt{\gamma_{EGC}} \\ &= \frac{1}{\sqrt{L}} \sum_{k=1}^{L} R_k. \end{aligned} \tag{3.15}$$

By definition, the MGF of h_{EGC} is

$$\begin{aligned} \mathcal{M}_{h_{EGC}}(s) &= \mathrm{E}\left[e^{-sh_{EGC}}\right] \\ &= \underbrace{\int_0^\infty \cdots \int_0^\infty}_{L} e^{-\frac{s}{\sqrt{L}}\sum_{k=1}^{L} r_k} f_{\mathbf{R}}(r_1, \ldots, r_L) dr_1 \ldots dr_L. \end{aligned} \tag{3.16}$$

If we apply the first-order joint PDF (3.8) to (3.16) and convert the L-fold integral to a product of L integrals we obtain $\mathcal{M}_{h_{EGC}}(s)$ for $s \to \infty$ as

$$\mathcal{M}_{h_{EGC}}(s) = \frac{e^{-\frac{\Lambda}{\Lambda+1}S^2}}{\det^{\frac{n}{2}}(\mathbf{M})} \left(\frac{2L^{\frac{n}{2}}\Gamma(n)}{\Gamma\left(\frac{n}{2}\right)}\right)^L \left(\prod_{k=1}^{L} \frac{1}{\sigma_k^2}\right)^{\frac{n}{2}} \frac{1}{s^{nL}} + o\left(\frac{1}{s^{nL}}\right). \tag{3.17}$$

Comparing (3.17) to (3.7) we find

$$a_{EGC} = \frac{e^{-\frac{\Lambda}{\Lambda+1}S^2}}{2\Gamma(nL)\det^{\frac{n}{2}}(\mathbf{M})} \left(\frac{2L^{\frac{n}{2}}\Gamma(n)}{\Gamma\left(\frac{n}{2}\right)}\right)^L \left(\prod_{k=1}^{L} \frac{1}{\sigma_k^2}\right)^{\frac{n}{2}} \tag{3.18}$$

and

$$t_{EGC} = \frac{nL}{2} - 1. \tag{3.19}$$

3.4.3 MRC

Since (2.16) is a linear sum, we can easily find the MGF of γ_{MRC} using (3.8) and convert the resulting the L-fold integral to a product of L easily evaluated integrals. This results in

$$\mathcal{M}_{\gamma_{MRC}}(s) = \frac{e^{-\frac{\Lambda}{\Lambda+1}S^2}}{\det^{\frac{n}{2}}(\mathbf{M})} \left(\prod_{k=1}^{L} \frac{1}{\sigma_k^2}\right)^{\frac{n}{2}} \frac{1}{s^{\frac{nL}{2}}} + o\left(\frac{1}{s^{\frac{nL}{2}}}\right) \tag{3.20}$$

for $s \to \infty$. From (3.6) and (3.20) parameters a and t can be calculated as

$$a_{MRC} = \frac{e^{-\frac{\Lambda}{\Lambda+1}S^2}}{\Gamma\left(\frac{nL}{2}\right) \det^{\frac{n}{2}}(\mathbf{M})} \left(\prod_{k=1}^{L} \frac{1}{\sigma_k^2}\right)^{\frac{n}{2}} \tag{3.21}$$

and

$$t_{MRC} = \frac{nL}{2} - 1. \tag{3.22}$$

3.5 Discussion and Numerical Results

3.5.1 Discussion

As the t parameter ($t+1$ is also known as the diversity gain and indicates the slope on a log-log plot of P_e^{∞} vs SNR) is identical for each diversity scheme we can directly evaluate the relative asymptotic error probability with identical modulation among the combining schemes solely by comparing the parameter a. It can be seen from (3.13), (3.18), and (3.21) that for each combining scheme, the parameters a_{SC}, a_{EGC}, and a_{MRC} share several common terms.

If we isolate the commonality, we can redefine a_{XX} as $a_{XX} = \mu_{XX}c$, where $c = \frac{e^{-\frac{\Lambda}{\Lambda+1}S^2}}{\det^{\frac{n}{2}}(\mathbf{M})}\left(\prod_{k=1}^{L}\frac{1}{\sigma_k^2}\right)^{\frac{n}{2}}$ is the common component among all combining schemes and μ_{XX} is the combining specific factor given by

$$\mu_{SC} = \frac{nL}{2\Gamma^L\left(\frac{n}{2}+1\right)} \tag{3.23}$$

$$\mu_{EGC} = \frac{1}{2\Gamma(nL)}\left[\frac{2L^{\frac{n}{2}}\Gamma(n)}{\Gamma\left(\frac{n}{2}\right)}\right]^L \tag{3.24}$$

$$\mu_{MRC} = \frac{1}{\Gamma\left(\frac{nL}{2}\right)}. \tag{3.25}$$

Note that μ_{XX} only depends on the severity of the fading and number of branches, and does not depend on the channel correlation or average branch power.

If we plot the μ_{XX} of SC and EGC relative to μ_{MRC} (the optimum linear combiner), i.e. μ_{MRC}/μ_{XX}, as in Fig. 3.1, we see that for dual diversity (L=2) and $n = 1$, SC and EGC achieve identical performance with $\mu_{SC} = \mu_{EGC} = 4/\pi$. This result has also been shown to apply at all SNRs for independent Nagakami-m fading channels [41]. For $L > 2$ and $n > 1$ we see that EGC is able to outperform SC while achieving similar performance to MRC. The performance gap between both SC and EGC relative to MRC increases with the number of branches and as the fading severity decreases.

Interestingly in Fig. 3.1, it appears as though as $n \to \infty$, the ratio μ_{MRC}/μ_{EGC} approaches a constant. This is indeed the case and can be

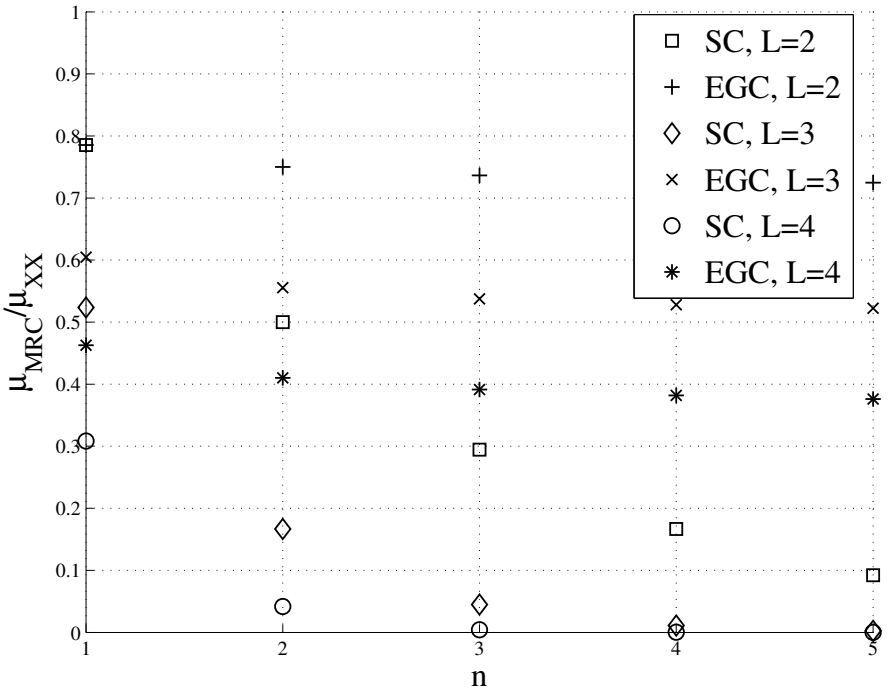

Figure 3.1: Performance of EGC and SC relative to MRC.

shown using Stirling's formula, $\lim_{x\to\infty}\Gamma(x) = \sqrt{2\pi}e^{-x}x^{x-1/2}$, to be

$$\lim_{n\to\infty}\frac{\mu_{MRC}}{\mu_{EGC}} = 2^{\frac{1-L}{2}}. \tag{3.26}$$

Also as $L \to \infty$ there is also a fixed relationship between the average SNR required for EGC and MRC to have equal performance. If $\bar{\gamma}_{EGC}$ and $\bar{\gamma}_{MRC}$ are the average SNR on each branch for EGC and MRC respectively, then

$$\frac{\bar{\gamma}_{EGC}}{\bar{\gamma}_{MRC}} = \left(\frac{\mu_{EGC}}{\mu_{MRC}}\right)^{\frac{2}{nL}}. \tag{3.27}$$

Again, using Sterling's formula, we obtain

$$\lim_{L\to\infty} \frac{\bar{\gamma}_{EGC}}{\bar{\gamma}_{MRC}} = \frac{e}{n2^{1-\frac{2}{n}}} \left[\frac{\Gamma(n)}{\Gamma\left(\frac{n}{2}\right)}\right]^{\frac{2}{n}} \tag{3.28}$$

$$= 10\log_{10}\left(\frac{e}{n2^{1-\frac{2}{n}}}\right) + \frac{20}{n}\log_{10}\left(\frac{\Gamma(n)}{\Gamma\left(\frac{n}{2}\right)}\right) \text{[dB]}. \tag{3.29}$$

This represents the additional power required at the transmitter if EGC is implemented over MRC to reduce the combiner complexity. Similar results for SC do not exist, with $\lim_{n\to\infty} \mu_{MRC}/\mu_{SC} = 0$ and $\lim_{L\to\infty} \bar{\gamma}_{SC}/\bar{\gamma}_{MRC} = \infty$.

3.5.2 Numerical Results

In order to validate our results we have plotted $P_{e,c}^{\infty}$ for BPSK and equal average branch SNR along with Monte Carlo simulations in Fig. 3.2, Fig. 3.3, and Fig. 3.4 for SC, EGC, and MRC respectively. In all cases we let $\lambda = [0.9, 0.3, 0.8]$. We can see from Figs. 3.2-3.4 that for each combining method the simulated results approach the asymptotic error rates as SNR increases.

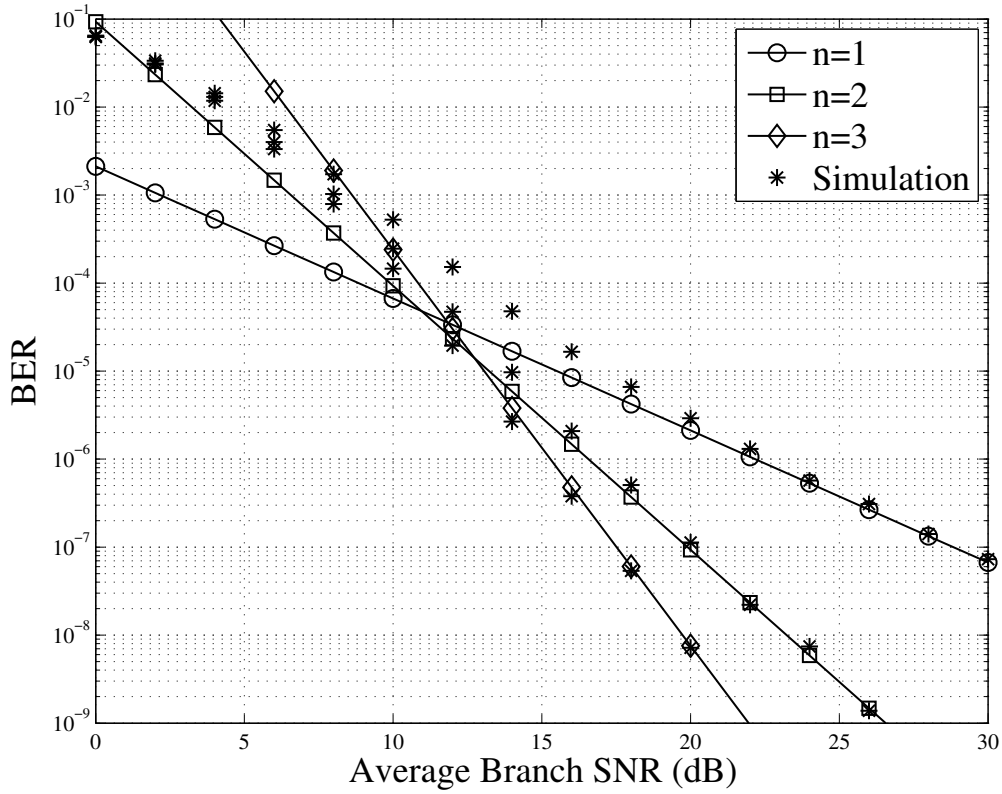

Figure 3.2: Asymptotic and simulated BERs of coherent BPSK of triple branch SC with generalized Rician fading channels with $S = 3$ and $\lambda = [0.9, 0.3, 0.8]$.

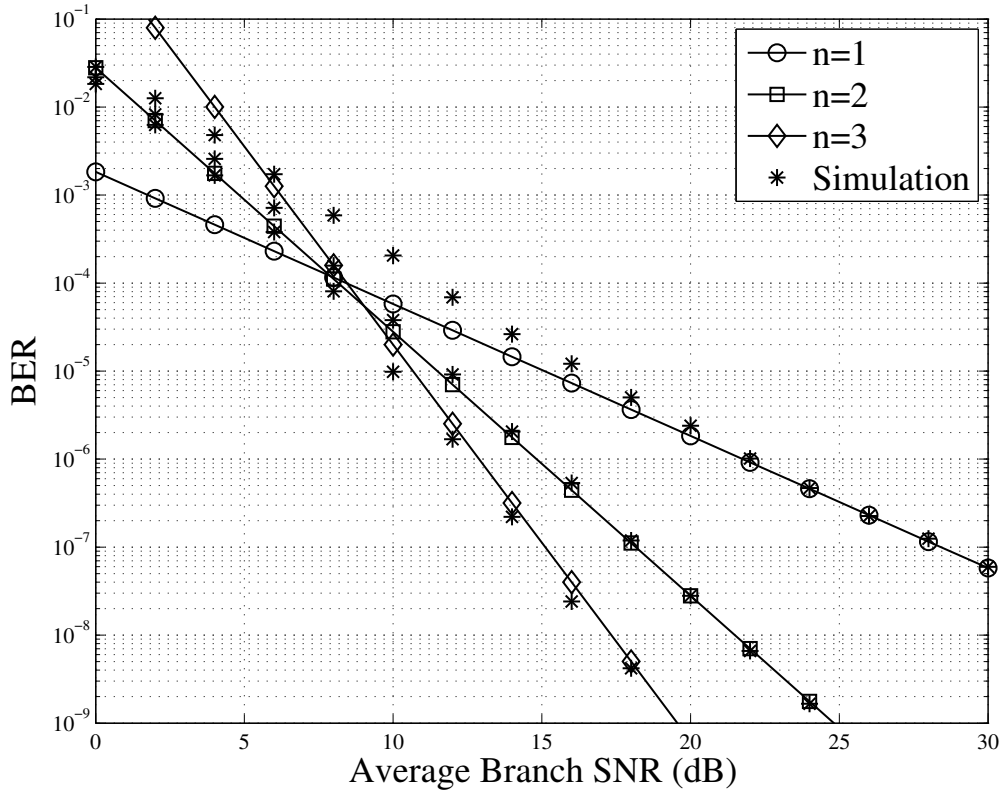

Figure 3.3: Asymptotic and simulated BERs of coherent BPSK of triple branch EGC with generalized Rician fading channels with $S = 3$ and $\lambda = [0.9, 0.3, 0.8]$.

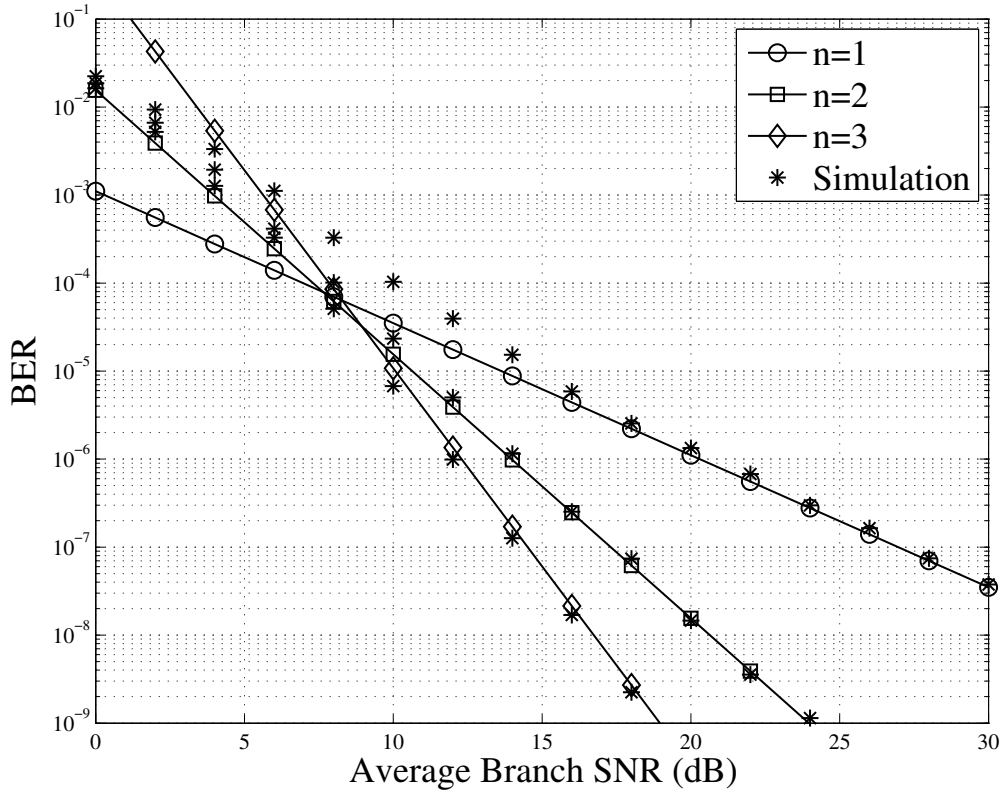

Figure 3.4: Asymptotic and simulated BERs of coherent BPSK of triple branch MRC with generalized Rician fading channels with $S = 3$ and $\lambda = [0.9, 0.3, 0.8]$.

Chapter 4

Exact Series Form of the BER with SC in Generalized Rician Fading

In this chapter we develop an exact infinite series representation for the PDF and CDF of the SNR for SC. The statistical distributions are then used to obtain an exact infinite series expression for the BER of binary coherent and noncoherent modulations. We also find an upper bound on the truncation error introduced when the infinite series is truncated to a finite number of terms.

4.1 Channel Model

Consider an L-branch diversity combiner where the transmitted signal is impaired by slow, frequency nonselective fading and AWGN on each branch. The instantaneous SNR on the kth branch is $\gamma_k = R_k^2$, where R_k is a generalized Rician RV. Assume correlation among branches fits the generalized

correlation model, then the average SNR on the kth branch is $\overline{\gamma}_k = \mathrm{E}[\gamma_k] = \sigma_k^2\left(\frac{n}{2} + \lambda_k^2 S^2\right)$ and the power correlation between the kth and ith branch is

$$\rho_{\gamma_k\gamma_i} = \frac{\lambda_k^2\lambda_i^2(\frac{n}{2} + 2S^2)}{\sqrt{\frac{n}{2} + 2\lambda_k^2 S^2}\sqrt{\frac{n}{2} + 2\lambda_i^2 S^2}}, \quad k \neq i \tag{4.1}$$

as found in Chapter 2. Furthermore, let the average SNR of the kth branch be given by $\bar{\gamma}_k = g_k\bar{\gamma}$ where g_k is the gain of the kth branch relative to some baseline SNR value $\bar{\gamma}$. For instance, $\bar{\gamma}$ could be the average SNR across all branches, in which case $\bar{\gamma} = \sum_{k=1}^{L}\bar{\gamma}_k$.

4.2 SNR Distribution

We start by deriving an infinite series expression for the CDF at the output of the SC combiner. Using the joint CDF of generalized Rician RVs with generalized correlation (2.27), the CDF of γ_{SC} is given in single integral form as

$$\begin{aligned} F_{\gamma_{SC}}(\gamma) =& F_{\mathbf{R}}\left(R_1 \leq \sqrt{\gamma}, R_2 \leq \sqrt{\gamma} \ldots, R_L \leq \sqrt{\gamma}\right) && (4.2)\\ =& \frac{\exp\left(-S^2\right)}{S^{\frac{n}{2}-1}} \int_0^{\infty} t^{\frac{n-2}{4}} \exp\left(-t\right) I_{\frac{n}{2}-1}(2S\sqrt{t}) \\ & \times \prod_{k=1}^{L}\left[1 - Q_{\frac{n}{2}}\left(\sqrt{\frac{2\lambda_k^2 t}{1-\lambda_k^2}}, \sqrt{\frac{2d_k\gamma}{\bar{\gamma}}}\right)\right] dt. && (4.3) \end{aligned}$$

where $d_k = \frac{(n+2\lambda_k^2 S^2)}{2g_k(1-\lambda_k^2)}$.

A novel infinite series form of the generalized Marcum Q-function in terms of generalized Laguerre polynomials was recently proposed by András *et al.* [42] as

$$Q_v(a,b) = 1 - \sum_{i=0}^{\infty} (-1)^i e^{-\frac{a^2}{2}} \frac{L_i^{(v-1)}\left(\frac{a^2}{2}\right)}{\Gamma(v+i+1)} \left(\frac{b^2}{2}\right)^{v+i}. \tag{4.4}$$

The availability of well known inequalities for the generalized Laguerre polynomial makes this series suitable for a truncation error analysis. Substituting (4.4) into (4.3) and interchanging the order of summation and integration we can express $F_{\gamma_{SC}}(\gamma)$ as an infinite series

$$F_{\gamma_{SC}}(\gamma) = \left[\prod_{k=1}^{L} d_k\right]^{\frac{n}{2}} \sum_{i=0}^{\infty} C_i \left(\frac{\gamma}{\bar{\gamma}}\right)^{i+\frac{nL}{2}} \tag{4.5}$$

where the coefficient C_i is given by

$$\begin{aligned} C_i =& \frac{(-1)^i e^{-S^2}}{S^{\frac{n}{2}-1}} \int_0^{\infty} t^{\frac{n-2}{4}} \exp\left(-\left(\Lambda+1\right)t\right) I_{\frac{n}{2}-1}\left(2S\sqrt{t}\right) \\ &\times \sum_{j_1+\cdots+j_L=i} \prod_{k=1}^{L} \frac{L_{j_k}^{\left(\frac{n}{2}-1\right)}\left(\frac{\lambda_k^2 t}{1-\lambda_k^2}\right)}{\Gamma(\frac{n}{2}+j_k+1)} d_k^{j_k} dt. \end{aligned} \tag{4.6}$$

To evaluate the integral in C_i we consider the integral identity

$$\int_0^{\infty} t^{i+\frac{\mu-1}{2}} e^{-\alpha t} I_{\mu-1}\left(2\beta\sqrt{t}\right) dt = i! \left(\frac{\beta}{\alpha^i}\right)^{\mu} \exp\left(\frac{\beta^2}{\alpha}\right) L_i^{(\mu-1)}\left(-\frac{\beta^2}{\alpha}\right) \tag{4.7}$$

where $i \in \mathbb{N}$ and $\mu > 0$. The derivation of (4.7) is located in Appendix B. The integral in C_i can then be evaluated using a finite series form of the generalized Laguerre polynomial [39, Eq. (22.3.9)]

$$L_i^{(\alpha)}(x) = \sum_{j=0}^{i} \frac{(j+\alpha+1)_{i-j}}{(i-j)!j!}(-x)^j, \quad \alpha > -1 \tag{4.8}$$

and the integral identity (4.7) along with some algebraic simplifications to obtain

$$\begin{aligned} C_i =& \frac{(-1)^i e^{-\frac{\Lambda}{\Lambda+1}S^2}}{(\Lambda+1)^{\frac{n}{2}}\Gamma^L\left(\frac{n}{2}\right)} \sum_{j_1+\cdots+j_L=i} \prod_{k=1}^{L} \frac{d_k^{j_k}}{j_k!\left(\frac{n}{2}+j_k\right)} \\ & \times \sum_{l_1=0,\ldots,l_L=0}^{j_1,\ldots,j_L} \frac{\left(\sum_{k=1}^{L} l_k\right)!}{(\Lambda+1)^{\sum_{k=1}^{L} l_k}} L_{\sum_{k=1}^{L} l_k}^{\left(\frac{n}{2}-1\right)}\left(-\frac{S^2}{1+\Lambda}\right) \\ & \times \prod_{k=1}^{L} \binom{j_k}{l_k} \frac{1}{\left(\frac{n}{2}\right)_{l_k}} \left(\frac{-\lambda_k^2}{1-\lambda_k^2}\right)^{l_k}. \end{aligned} \tag{4.9}$$

The PDF of γ_{SC} can be found by differentiating (4.5) w.r.t. γ, upon which we obtain

$$f_{\gamma_{SC}}(\gamma) = \left[\prod_{k=1}^{L} d_k\right]^{\frac{n}{2}} \sum_{i=0}^{\infty} \left(\frac{nL}{2}+i\right) C_i \bar{\gamma} \left(\frac{\gamma}{\bar{\gamma}}\right)^{i+\frac{nL}{2}-1}. \tag{4.10}$$

It is easy to verify that the first term in (4.10) is the asymptotic PDF at the output of the SC combiner (3.12) derived in Chapter 3.

As a sanity check, we examine the special case when $L = 1$. For $L = 1$,

C_i is simplifies to

$$\begin{aligned} C_i =& \frac{(-d)^i(1-\lambda^2)^{\frac{n}{2}+i}e^{-\lambda^2S^2}}{\Gamma\left(\frac{n}{2}\right)i!\left(\frac{n}{2}+i\right)}\sum_{l=0}^{i}\binom{i}{l}\left(1+\frac{\lambda^2}{1-\lambda^2}\right)^{i-l}\left(\frac{-\lambda^2}{1-\lambda^2}\right)^{l} \\ & \times \frac{L_l^{\left(\frac{n}{2}-1\right)}(-(1-\lambda^2)S^2)}{L_l^{\left(\frac{n}{2}-1\right)}(0)} \\ =& \frac{(-d)^i(1-\lambda^2)^{\frac{n}{2}+i}e^{-\lambda^2S^2}}{\Gamma\left(\frac{n}{2}\right)i!\left(\frac{n}{2}+i\right)}\frac{L_i^{\left(\frac{n}{2}-1\right)}(\lambda^2S^2)}{L_i^{\left(\frac{n}{2}-1\right)}(0)} \end{aligned} \tag{4.11}$$

where we have used the fact that $L_n^{(\alpha)}(0) = \frac{(\alpha+1)_n}{n!}$ and a Laguerre sum formula [43, Eq. (18.18.12)]. Substituting (4.11) into (4.10) we obtain the following

$$f_{\gamma_{SC}}(\gamma) = \frac{e^{-\lambda^2S^2}}{\Gamma\left(\frac{n}{2}\right)\sigma^2}\left(\frac{\gamma}{\sigma^2}\right)^{\frac{n}{2}-1}\sum_{i=0}^{\infty}\left(-\frac{\gamma}{\sigma^2}\right)^{i}\frac{L_i^{\left(\frac{n}{2}-1\right)}(\lambda^2S^2)}{i!L_i^{\left(\frac{n}{2}-1\right)}(0)} \tag{4.12}$$

$$= \frac{\gamma^{\frac{n-2}{4}}e^{-\lambda^2S^2-\frac{\gamma}{\sigma^2}}}{\sigma^2\left(\lambda S\sigma\right)^{\frac{n}{2}-1}}I_{\frac{n}{2}-1}\left(\frac{2\lambda S}{\sigma}\sqrt{\gamma}\right) \tag{4.13}$$

where we have used the formula [42]

$$\sum_{i=0}^{\infty}\frac{L_i^{(\alpha)}(x)}{L_i^{(\alpha)}(0)}\frac{(-z)^i}{i!} = \Gamma(\alpha+1)e^{-z}(xz)^{-\frac{\alpha}{2}}I_\alpha(2\sqrt{xz}). \tag{4.14}$$

This matches the result found by differentiating (4.2) w.r.t. γ, substituting (2.29) and letting $L = 1$.

4.3 BER of Binary Modulations

4.3.1 BER for Binary Coherent Modulations

For binary coherent modulations, the conditional error rate is given by

$$P_{e|\gamma} = Q\left(\sqrt{q\gamma}\right). \tag{4.15}$$

where $q = 2$ for BPSK and $q = 1$ for binary coherent frequency shift keying (BCFSK). Substituting (4.15) into (3.2) and changing the order of integration we obtain

$$P_{e,c} = \frac{1}{\sqrt{2\pi}} \int_0^\infty \exp\left(-\frac{x^2}{2}\right) F_\gamma\left(\frac{x^2}{q}\right) dx. \tag{4.16}$$

An infinite series form for $P_{e,c}$ can then be found by substituting (4.5) into (4.16) and changing the order of summation and integration to arrive at

$$P_{e,c} = \frac{1}{2\sqrt{\pi}} \left[\prod_{k=1}^{L} d_k\right]^{\frac{n}{2}} \sum_{i=0}^{\infty} \frac{2^{\frac{nL}{2}+i} C_i \Gamma\left(i + \frac{nL+1}{2}\right)}{(\bar{\gamma} q)^{\frac{nL}{2}+i}}. \tag{4.17}$$

As $\bar{\gamma} \to \infty$, Eq. (4.17) is dominated by the first term in the summation:

$$P_{e,c} \approx \frac{1}{2\sqrt{\pi}} \prod_{k=1}^{L} \left(\frac{n + 2\lambda_k^2 S^2}{2g_k}\right)^{\frac{n}{2}} \frac{(-1)^i e^{-\frac{\Lambda}{\Lambda+1} S^2} \Gamma\left(\frac{nL+1}{2}\right)}{(\Lambda+1)^{\frac{n}{2}} \Gamma^L\left(\frac{n}{2}+1\right)} \frac{1}{\bar{\gamma}^{\frac{nL}{2}}} \tag{4.18}$$

which matches the asymptotic BER (3.4) when t and a are given by (3.14) and (3.13) respectively.

Although we have only derived the BER of coherent binary modulations,

the results can be generalized to many M-ary linear digital modulations following an MGF approach [1].

4.3.2 BER for Binary Noncoherent Modulations

As mentioned in Chapter 3, the conditional error rate for binary noncoherent modulations is given by $P_{e|\gamma} = \frac{1}{2}\exp(-q\gamma)$, where $q = 1/2$ for BNCFSK and $q = 1$ for BDPSK. We then obtain the average BER as

$$P_{e,nc} = \frac{1}{2}\int_0^\infty \exp(-q\gamma)\, f_\gamma(\gamma)\, d\gamma. \tag{4.19}$$

Substituting (4.10) into (4.19) and changing the order of integration we obtain an infinite series solution for the BER

$$P_{e,nc} = \frac{1}{2}\left[\prod_{k=1}^{L} d_k\right]^{\frac{n}{2}} \sum_{i=0}^{\infty} \frac{C_i \Gamma\left(i + \frac{nL}{2} + 1\right)}{(\bar{\gamma}q)^{\frac{nL}{2}+i}}. \tag{4.20}$$

4.4 Convergence and Truncation Error

4.4.1 Convergence

Thus far, we have proceeded with interchanging the order of summation and integration without considering whether the resulting series converges or not. While we will show the infinite series forms of $F_{\gamma_{SC}}(\gamma)$ and $f_{\gamma_{SC}}(\gamma)$ are convergent for all $0 \leq \gamma < \infty$, the infinite series for the BER for both

coherent and noncoherent modulations are only convergent for a sufficiently high average SNR.

We start by finding an upper bound on C_i. To achieve this, we return to the form of C_i prior to carrying out the integration (4.6), and apply a well known inequality for the generalized Laguerre polynomial [39, Eq. (22.14.13)]

$$\left|L_i^{(\alpha)}(x)\right| \leq \frac{(\alpha+1)_i}{i!}\exp\left(\frac{x}{2}\right), \quad \alpha \geq 0, x \geq 0 \tag{4.21}$$

along with an integral identity [37, Eq. (3.15.2.8)] to obtain

$$\begin{aligned}
|C_i| &\leq \frac{\exp\left(-\frac{\Lambda S^2}{(\Lambda+2)}\right)}{\Gamma^L\left(\frac{n}{2}\right)\left(\frac{\Lambda}{2}+1\right)^{\frac{n}{2}}} \sum_{j_1+\cdots+j_L=i} \prod_{k=1}^{L} \frac{d_k^{j_k}}{\left(\frac{n}{2}+j_k\right) j_k!} \\
&\leq \frac{\exp\left(-\frac{\Lambda S^2}{(\Lambda+2)}\right)}{\Gamma^L\left(\frac{n}{2}+1\right)\left(\frac{\Lambda}{2}+1\right)^{\frac{n}{2}}} \sum_{j_1+\cdots+j_L=i} \prod_{k=1}^{L} \frac{d_k^{j_k}}{j_k!} \\
&= \frac{\exp\left(-\frac{\Lambda S^2}{(\Lambda+2)}\right)}{\Gamma^L\left(\frac{n}{2}+1\right)\left(\frac{\Lambda}{2}+1\right)^{\frac{n}{2}}} \frac{\eta^i}{i!}
\end{aligned} \tag{4.22}$$

where $\eta = \sum_{k=1}^{L} d_k$ and we have used the multinomial identity to get (4.22). Note that due to the use of (4.21), which is valid only for $\alpha \geq 0$, Eq. (4.22) applies for $n > 1$ only. For $n = 1$ we use the inequality

$$\left|L_i^{(\alpha)}(x)\right| \leq 2\exp\left(\frac{x}{2}\right) \quad -1 < \alpha \leq 0,\ x \geq 0 \tag{4.23}$$

which is a relaxed form of [39, Eq. (22.14.14)]. Using a similar methodology

to how (4.25) was obtained, we find for $n = 1$

$$\begin{aligned}
|C_i| \leq & \frac{2^L \exp\left(-\frac{\Lambda S^2}{(\Lambda+2)}\right)}{\sqrt{\frac{\Lambda}{2}+1}} \sum_{j_1+\cdots+j_L=i} \prod_{k=1}^{L} \frac{d_k^{j_k}}{\Gamma(j_k+\frac{3}{2})} \\
\leq & \frac{2^L \exp\left(-\frac{\Lambda S^2}{(\Lambda+2)}\right)}{\sqrt{\frac{\Lambda}{2}+1}} \sum_{j_1+\cdots+j_L=i} \prod_{k=1}^{L} \frac{d_k^{j_k}}{j_k!} \\
= & \frac{2^L \exp\left(-\frac{\Lambda S^2}{(\Lambda+2)}\right)}{\sqrt{\frac{\Lambda}{2}+1}} \frac{\eta^i}{i!}.
\end{aligned} \tag{4.24}$$

Since (4.22) and (4.24) vary only by a constant coefficient, we define a new term valid for all $n = 1, 2, \ldots$

$$|C_i| \leq A\frac{\eta^i}{i!} \tag{4.25}$$

$$A = \begin{cases} \frac{2\exp\left(-\frac{\Lambda S^2}{(\Lambda+2)}\right)}{\pi^{\frac{L}{2}}\left(\frac{\Lambda}{2}+1\right)^{\frac{n}{2}}} & n = 1 \\ \frac{\exp\left(-\frac{\Lambda S^2}{(\Lambda+2)}\right)}{\Gamma^L\left(\frac{n}{2}+1\right)\left(\frac{\Lambda}{2}+1\right)^{\frac{n}{2}}} & n = 2, 3, \ldots \end{cases}. \tag{4.26}$$

Using (4.25), we can now bound the series form of $F_{\gamma_{SC}}(\gamma)$ (4.5) as follows

$$\begin{aligned}
|F_{\gamma_{SC}}(\gamma)| \leq & \left[\prod_{k=1}^{L} d_k\right]^{\frac{n}{2}} \sum_{i=0}^{\infty} |C_i| \left(\frac{\gamma}{\bar{\gamma}}\right)^{i+\frac{nL}{2}} \\
\leq & A\left(\frac{\gamma}{\bar{\gamma}}\right)^{\frac{nL}{2}} \left[\prod_{k=1}^{L} d_k\right]^{\frac{n}{2}} \sum_{i=0}^{\infty} \frac{1}{i!} \left(\frac{\eta\gamma}{\bar{\gamma}}\right)^{i} \\
= & A\left(\frac{\gamma}{\bar{\gamma}}\right)^{\frac{nL}{2}} \left[\prod_{k=1}^{L} d_k\right]^{\frac{n}{2}} \exp\left(\frac{\eta\gamma}{\bar{\gamma}}\right).
\end{aligned} \tag{4.27}$$

Eq. (4.27) converges for $0 \leq \gamma < \infty$, thus convergence of (4.5) is guaranteed for the same interval. A similar exercise can be performed to show that the PDF in (4.10) also converges for $0 \leq \gamma < \infty$.

Due to the presence of the $\Gamma(\cdot)$ term in the numerator of the summation in (4.17), convergence of the series is conditional. Finding the entire region of convergence of (4.17) is extremely complex due to the nested summations. However, we can find a subset of the region of convergence using the upper bound on $|C_i|$. Using (4.25), we find

$$|P_{e,c}| \leq \frac{2^{\frac{nL}{2}-1}A}{\sqrt{\pi}(q\bar{\gamma})^{\frac{nL}{2}}} \left[\prod_{k=1}^{L} d_k\right]^{\frac{n}{2}} \sum_{i=0}^{\infty} \frac{\Gamma\left(i + \frac{(nL+1)}{2}\right)}{i!} \left(\frac{2\eta}{q\bar{\gamma}}\right)^{i} \tag{4.28}$$

which converges by the ratio test for $\frac{2\eta}{q\bar{\gamma}} < 1$. Similarly, it can be shown (4.20) converges when $\frac{\eta}{q\bar{\gamma}} < 1$.

The requirement $\frac{2\eta}{q\bar{\gamma}} < 1$ or $\frac{\eta}{q\bar{\gamma}} < 1$ is satisfied provided that average branch power is sufficiently high. For instance, for branches experiencing equally correlated Nakagami-m fading, equal average branch SNR, and BPSK modulation we require $\frac{\eta}{\bar{\gamma}} < 1$, which is achieved when $\bar{\gamma} > \frac{mL}{(1-\sqrt{\rho})}$ where $\rho = \lambda^4$ is the power correlation coefficient between any two branches. From this we can infer that the minimum $\bar{\gamma}$ required to guarantee the infinite series expressions for P_e converge increases with the number of branches and branch correlation, but decreases with the fading severity.

4.4.2 Truncation Error

In this section we derive an upper bound on the truncation errors when the infinite series for SNR CDF (4.5) and BER for binary coherent modulations (4.17) are terminated at a finite number of terms. We omit the results for binary noncoherent modulations, but the truncation error can be bounded in a similar manner.

The truncation of (4.5) and (4.17) and to the first $N+1$ terms is given by

$$\hat{F}_{\gamma_{SC}}^{(N)}(\gamma) = \left[\prod_{k=1}^{L} d_k\right]^{\frac{n}{2}} \sum_{i=0}^{N} C_i \left(\frac{\gamma}{\bar{\gamma}}\right)^{i+\frac{nL}{2}} \tag{4.29}$$

$$\hat{P}_{e,c}^{(N)} = \frac{1}{2\sqrt{\pi}} \left[\prod_{k=1}^{L} d_k\right]^{\frac{n}{2}} \sum_{i=0}^{N} \frac{2^{\frac{nL}{2}+i} C_i \Gamma\left(i+\frac{nL+1}{2}\right)}{(q\bar{\gamma})^{\frac{nL}{2}+i}}. \tag{4.30}$$

We then define the associated truncation errors as $\epsilon_{F_{\gamma_{SC}}}^{(N)}(\gamma) \triangleq \left|F_{\gamma_{SC}}(\gamma) - \hat{F}_{\gamma_{SC}}^{(N)}(\gamma)\right|$ and $\epsilon_{P_{e,c}}^{(N)}(\gamma) \triangleq \left|P_{e,c}(\gamma) - \hat{P}_{e,c}^{(N)}(\gamma)\right|$ respectively. $\epsilon_{F_{\gamma_{SC}}}^{(N)}(\gamma)$ can be bounded using (4.25) to obtain

$$\epsilon_{F_{\gamma_{SC}}}^{(N)}(\gamma) \leq A\left(\frac{\gamma}{\bar{\gamma}}\right)^{\frac{nL}{2}} \left[\prod_{k=1}^{L} d_k\right]^{\frac{n}{2}} \sum_{i=N+1}^{\infty} \frac{1}{i!}\left(\frac{\eta\gamma}{\bar{\gamma}}\right)^{i} \tag{4.31}$$

$$= A\left(\frac{\gamma}{\bar{\gamma}}\right)^{\frac{nL}{2}} \left[\prod_{k=1}^{L} d_k\right]^{\frac{n}{2}} \left\{\exp\left(\frac{\eta\gamma}{\bar{\gamma}}\right)^{i} - \sum_{i=0}^{N} \frac{1}{i!}\left(\frac{\eta\gamma}{\bar{\gamma}}\right)^{i}\right\}. \tag{4.32}$$

Likewise we bound $\epsilon_{P_{e,c}}^{(N)}(\gamma)$ as

$$\epsilon_{P_{e,c}}^{(N)} \leq \frac{2^{\frac{nL}{2}-1}A}{\sqrt{\pi}(q\bar{\gamma})^{\frac{nL}{2}}}\left[\prod_{k=1}^{L} d_k\right]^{\frac{n}{2}} \sum_{i=N+1}^{\infty} \frac{\Gamma\left(i+\frac{nL+1}{2}\right)}{i!}\left(\frac{2\eta}{q\bar{\gamma}}\right)^{i} \tag{4.33}$$

$$= \frac{2^{\frac{nL}{2}-1}\Gamma\left(\frac{nL+1}{2}\right)A}{\sqrt{\pi}(q\bar{\gamma})^{\frac{nL}{2}}}\left[\prod_{k=1}^{L} d_k\right]^{\frac{n}{2}} \left\{\frac{1}{\left(1-\frac{2\eta}{q\bar{\gamma}}\right)^{\frac{nL+1}{2}}} - \sum_{i=0}^{N} \frac{\left(\frac{nL+1}{2}\right)_i}{i!}\left(\frac{2\eta}{q\bar{\gamma}}\right)^{i}\right\} \tag{4.34}$$

where we have used the binomial series $\frac{1}{(1-x)^{\alpha}} = \sum_{i=0}^{\infty} \frac{(\alpha)_i}{i!}x^i,\ |x| < 1$ to obtain (4.34). It is easy to see from (4.33) that the upper bound on the truncation error is $o\left(\bar{\gamma}^{-\left(\frac{nL}{2}+N+2\right)}\right)$, the same order as the first term ignored when the series is truncated to (4.30). Thus, we can conclude our truncation error bound decreases relative to the truncated error rate as $\bar{\gamma} \to \infty$.

4.5 Numerical Results

In order to verify that (4.30) converges to the exact error rate, we have plotted it for BPSK with $N = 30$ along with Monte Carlo simulations for Nakagami-m ($m = 2$) and Rician ($S = 1.5$) fading with equal average branch SNR in Fig. 4.1. In both cases we have used $\lambda = [0.6, 0.4, 0.9]$, resulting in

power correlation matrices, where the (k,i)th element is given by (4.1), of

$$\mathbf{P}_1 = \begin{pmatrix} 1 & 0.149 & 0.460 \\ 0.149 & 1 & 0.252 \\ 0.460 & 0.252 & 1 \end{pmatrix} \tag{4.35}$$

and

$$\mathbf{P}_2 = \begin{pmatrix} 1 & 0.058 & 0.292 \\ 0.058 & 1 & 0.130 \\ 0.292 & 0.130 & 1 \end{pmatrix} \tag{4.36}$$

for Rician and Nagakami-m respectively. We see fem Fig. 4.1 that in both cases, the approximation is highly accurate where the series converges. The convergence criterion for BPSK, $\frac{\eta}{\bar{\gamma}} < 1$, is satisfied when $\bar{\gamma} > 12.85$ dB for Rician fading and $\bar{\gamma} > 12.05$ dB for Nakagami-m fading. This is very close to the true value for the Nakagami-m fading; however, the convergence region of Rician fading is underestimated by roughly 2 dB.

Although we have chosen $N = 30$ in the previous example, the asymptotic error rate can be greatly improved by including only a couple extra terms. This is shown in Fig. 4.2, where we have replotted the asymptotic ($N = 0$) error rate along with $N = 1$ and $N = 2$ for Rician fading. The parameters are the same as the for the Rician case in Fig. 4.1. The asymptotic error rate is not within 1% of the exact error rate until 28.9 dB. By adding a single additional term this occurs at 18.5 dB, and two additional terms improves it further to 14.8 dB. Thus, we can extend the SNR region where the asymptotic

expression is valid with little additional complexity by including the first several terms of the infinite series.

Fig. 4.3 shows the relative truncation error for Nakagami-2 fading, where the relative truncation error is the ratio of (4.34) to (4.30). As we would expect, the number of terms required to satisfy a truncation error target diminishes as SNR increases. For instance, to guarantee a relative truncation error less than 1%, we require $N = 40$ at 14.3 dB, but this drops to $N = 10$ at 17.4 dB, and further to $N = 5$ at 19.7 dB. Although it is tempting to increase N to achieve an arbitrary accuracy, computation of C_N can be very intensive for large N and numerical integration of (4.16) may be more efficient. However, it should be noted that provided the relative SNRs between branches remains constant, $C_i,\ i = 1, 2, \ldots, N$ need only be computed once, whereas numerical integration would have to be performed at each SNR.

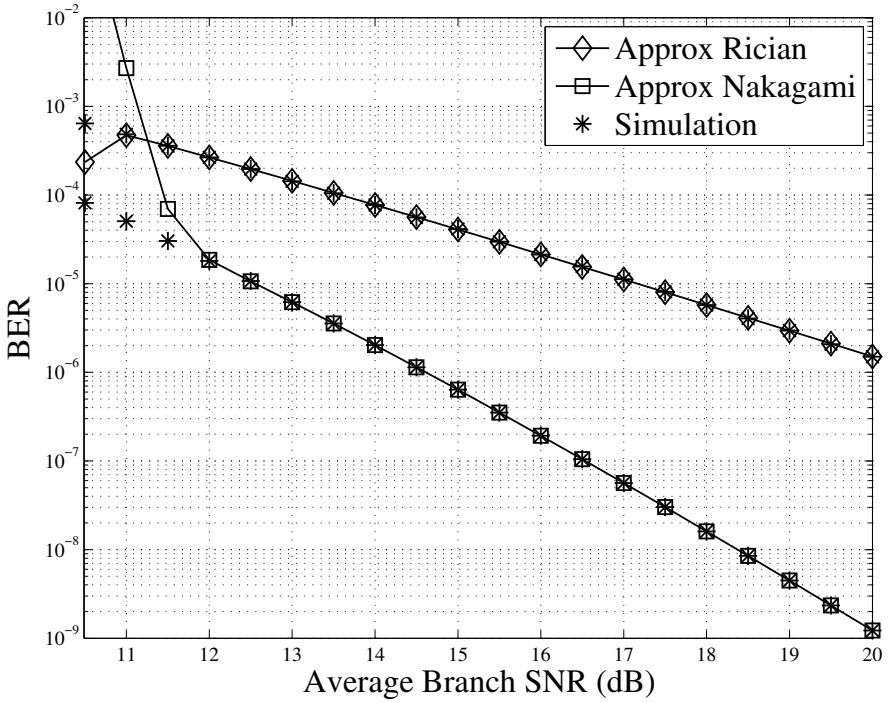

Figure 4.1: Approximate ($N = 30$) and simulated BERs of coherent BPSK of triple branch SC with Rician and Nakagami-m fading. Average SNR is identical for each branch. For Rician fading, $S = 1.5$ and for Nakagami-m, $m = 2$. Power correlation is according to $\mathbf{P}_1$ and $\mathbf{P}_2$ for Rician and Nakagami-m, respectively.

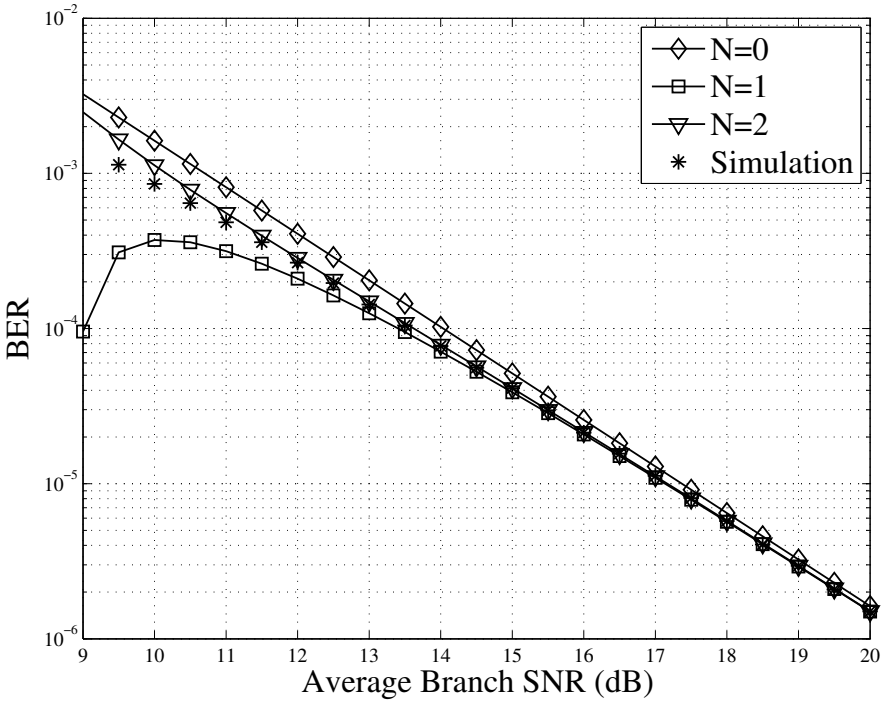

Figure 4.2: Approximate and simulated BERs of coherent BPSK of triple branch SC with Rician fading ($S = 1.5$) and equal average branch SNR. Branches are correlated with power correlation matrix $\mathbf{P}_1$.

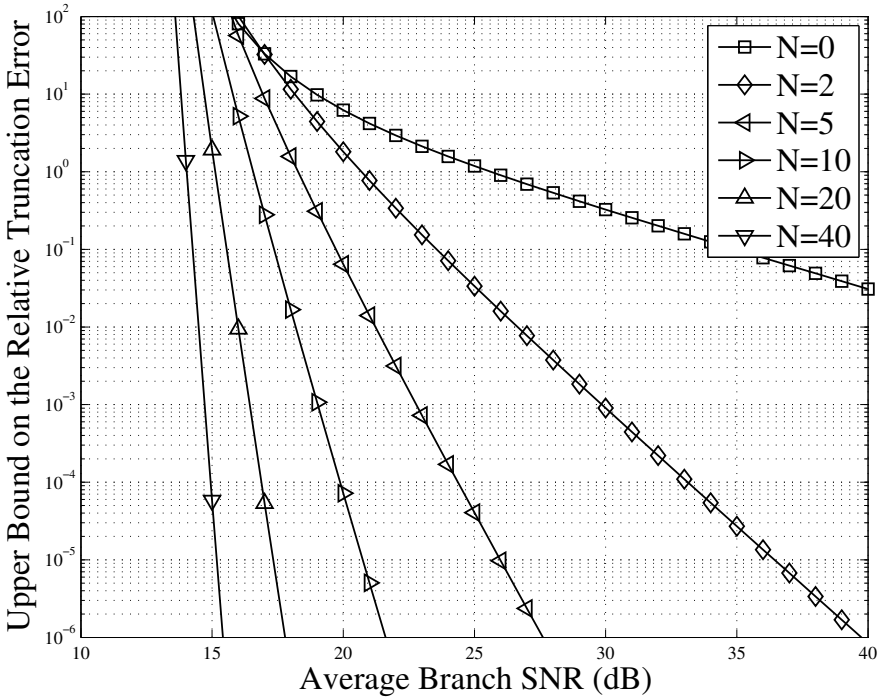

Figure 4.3: Relative truncation error for coherent BPSK with triple branch SC in Nakagami-2 fading and equal average branch SNR. Branches are correlated with power correlation matrix $\mathbf{P}_2$.

Chapter 5

Asymptotically Tight Error Bounds for EGC with Generalized Rician Fading

In this chapter, we derive single integral upper and lower bounds on the average error rate of a receiver employing EGC in correlated generalized Rician fading. These bounds are asymptotically exact, i.e. as average SNR approaches infinity. Furthermore, the bounds reduce to the exact error rate when the branches are independent.

5.1 Channel Model

Consider an L-branch diversity combiner where the transmitted signal is impaired by slow, frequency nonselective fading and AWGN on each branch. The instantaneous SNR on the kth branch is $\gamma_k = R_k^2$, where R_k is a generalized Rician RV. Assume correlation among branches fits the generalized correlation model, then the average SNR on the kth branch is $\overline{\gamma}_k = \mathrm{E}[\gamma_k] =$

$\sigma_k^2\left(\frac{n}{2}+\lambda_k^2 S^2\right)$ and power correlation between the kth and ith branch is

$$\rho_{\gamma_k\gamma_i}=\frac{\lambda_k^2\lambda_i^2(\frac{n}{2}+2S^2)}{\sqrt{\frac{n}{2}+2\lambda_k^2S^2}\sqrt{\frac{n}{2}+2\lambda_i^2S^2}},\quad k\neq i \tag{5.1}$$

as found in Chapter 2.

5.2 Bounds on Joint PDF

We first find bounds on the joint PDF of the generalized Rician distributed fading amplitudes $\mathbf{R}=[R_1,R_2,\ldots,R_L]$. As derived in Chapter 2, the joint PDF is given by

$$\begin{aligned}f_{\mathbf{R}}(r_1,r_2,\ldots,r_L)=&\frac{\exp\left(-S^2\right)}{S^{\frac{n}{2}-1}}\int_0^\infty t^{\frac{n-2}{4}}\exp\left(-t\right)I_{\frac{n}{2}-1}(2S\sqrt{t})\\&\times\prod_{k=1}^{L}\frac{r_k^{\frac{n}{2}}}{\left(\lambda_k^2\sigma_k^2t\right)^{\frac{n-2}{4}}\Omega_k^2}\exp\left\{-\frac{r_k^2+\lambda_k^2\sigma_k^2t}{2\Omega_k^2}\right\}I_{\frac{n}{2}-1}\left(\frac{r_k\sqrt{\sigma_k^2\lambda_k^2t}}{\Omega_k^2}\right)dt\end{aligned} \tag{5.2}$$

where $\Omega_k^2=\frac{1}{2}\sigma_k^2(1-\lambda_k^2)$. In order for these bounds to be asymptotically exact, we must preserve the shape of (5.2) at the origin, that is as $\frac{r_k^2}{\bar{\gamma}_k}\to 0$ or equivalently as $\frac{r_k^2}{\sigma_k^2}\to 0$. However, the bounds must also satisfy two additional objectives in order to provide a meaningful reduction of computational burden over the exact analysis. The first, and the most obvious one, is to simplify (5.2) by removing the integral over t. The impediment to finding a closed form solution of this integral is the product of Bessel

functions. Thus, a key component of our derivations is that both upper and lower bounds of the Bessel function approach equality at the origin in order to preserve the asymptotic behaviour. The second objective is that the joint PDF bounds must appear as those of independent RVs, i.e. as $f_{\mathbf{R}}(r_1, r_2, \ldots, r_L) \lessgtr A \prod_{k=1}^{L} W(r_k)$, where A is some constant term. This allows for bounds on the CHF, which we use to find the average error rate via well known methods, to be found as $A \prod_{k=1}^{L} \Phi_W$, where Φ_W is the CHF of W.

5.2.1 Lower Bound

A simple lower bound on $I_v(x)$ can be found by observing that each term in its series expansion,

$$I_v(x) = \left(\frac{1}{2}x\right)^v \sum_{i=0}^{\infty} \frac{\left(\frac{1}{2}x\right)^{2i}}{i!\Gamma(v+i+1)} \tag{5.3}$$

is positive when $v \geq -\frac{1}{2},\ x \geq 0$. Thus, we can lower bound the modified Bessel function by truncating the series expansion to the first term, i.e.

$$I_v(x) \geq \frac{1}{\Gamma(v+1)} \left(\frac{1}{2}x\right)^v,\ v \geq -\frac{1}{2}, x \geq 0. \tag{5.4}$$

As it is the first term in the series expansion, Eq. (5.4) approaches equality as $x \to 0$. Substituting (5.4) into (5.2) and using the integral identity [37,

Eq. (3.15.2.8)] we obtain

$$f_{\mathbf{R}}(r_1,\ldots,r_L) \geq \frac{e^{-\frac{\Lambda}{\Lambda+1}S^2}}{\det^{\frac{n}{2}}(\mathbf{M})} \prod_{k=1}^{L} \frac{2r_k^{n-1}}{\Gamma\left(\frac{n}{2}\right)\sigma_k^n} e^{-\frac{r_k^2}{2\Omega_k^2}} \tag{5.5}$$

where $\Lambda = \sum_{k=1}^{L} \frac{\lambda_k^2}{1-\lambda_k^2}$ and the matrix $\mathbf{M}$ is defined in (3.9). Eq. (5.5) satisfies both our objectives, and thus it is a suitable lower bound.

For the special case of Nakagami-m fading, we note that (5.5) is a scaled product of Nakagami-m PDFs

$$f_{\mathbf{R}}(r_1,\ldots,r_L) \geq \frac{1}{(1+\Lambda)^m} \prod_{k=1}^{L} \frac{2^{1-m} r_k^{2m-1}}{\Gamma(m)\,\Omega_k^{2m}} e^{-\frac{r_k^2}{2\Omega_k^2}} \tag{5.6}$$

and thus the equality is also achieved for independent branches since $\Lambda = 0$.

5.2.2 Upper Bound

While derivation of a suitable lower bound of the joint PDF is straightforward, this is not the case for the upper bound. We start by considering an upper bound on the Bessel function of the first kind [39, Eq. (9.1.62)]

$$|J_v(x)| \leq \frac{\exp|\Im(x)|}{\Gamma(v+1)} \left|\frac{1}{2}x\right|,\ v \geq -\frac{1}{2}. \tag{5.7}$$

Using the relation $I_v(x) = j^{-v}J_v(jx)$, where $j^2 = -1$, we obtain for $x \in \mathbb{R}$

$$I_v(x) \leq \frac{\exp(x)}{\Gamma(v+1)} \left(\frac{1}{2}x\right)^v,\ v \geq -\frac{1}{2}, x \geq 0 \tag{5.8}$$

which approaches equality as $x \to 0$. Substituting (5.8) into (5.2) we obtain an upper bound on $f_{\mathbf{R}}(r_1, \ldots, r_L)$ as

$$f_{\mathbf{R}}(r_1, \ldots, r_L) \leq G_1 \prod_{k=1}^{L} \frac{2r_k^{n-1}}{\Gamma(\frac{n}{2}) 2^{\frac{n}{2}} \Omega_k^n} \exp\left(-\frac{r_k^2}{2\Omega_k^2}\right) \tag{5.9}$$

where

$$G_1 = \frac{2\exp(-S^2)}{S^{\frac{n-2}{2}}} \int_0^\infty t^{\frac{n}{2}} \exp\left(-(1+\Lambda)t^2 + \sum_{k=1}^{L} \frac{r_k \sqrt{\sigma_k^2 \lambda_k^2}}{\Omega_k^2} t\right) I_{\frac{n}{2}-1}(2St) dt \tag{5.10}$$

and we have also made the integral substitution t^2 for t. If we define $u = \sum_{k=1}^{L} \frac{r_k \sqrt{\sigma_k^2 \lambda_k^2}}{2\sqrt{1+\Lambda}\Omega_k^2}$, and make the integral substitution $z = \sqrt{1+\Lambda}t - u$, we arrive at an expression for G_1 which can be split into two integrals G_2 and G_3 as

$$\begin{aligned} G_1 = & \frac{\exp(u^2 - S^2)}{S^{\frac{n}{2}-1}(1+\Lambda)^{\frac{n}{4}+\frac{1}{2}}} \Bigg[\underbrace{2\int_{-u}^{0} (z+u)^{\frac{n}{2}} \exp\left(-z^2\right) I_{\frac{n}{2}-1}\left(\frac{2S(z+u)}{\sqrt{1+\Lambda}}\right) dz}_{G_2} \\ & + \underbrace{2\int_{0}^{\infty} (z+u)^{\frac{n}{2}} \exp\left(-z^2\right) I_{\frac{n}{2}-1}\left(\frac{2S(z+u)}{\sqrt{1+\Lambda}}\right) dz}_{G_3} \Bigg]. \end{aligned} \tag{5.11}$$

The term G_2 can be upper bounded by observing that the integrand is maximized when $z = 0$, and we get

$$G_2 \leq 2u^{\frac{n}{2}+1} I_{\frac{n}{2}-1}\left(\frac{2Su}{\sqrt{1+\Lambda}}\right). \tag{5.12}$$

Applying the Bessel function inequality in (5.8) to (5.12), we arrive at a suitable upper bound for G_2 as

$$G_2 \leq \frac{2u^n}{\Gamma\left(\frac{n}{2}\right)} \left(\frac{S}{\sqrt{1+\Lambda}}\right)^{\frac{n}{2}-1} \exp\left(\frac{2Su}{\sqrt{1+\Lambda}}\right). \tag{5.13}$$

Let us now consider G_3. The integral in G_3 cannot be expressed in closed form due to the linear shift of the integrand by u in the power term and Bessel function. Using the fact that $x^{-v} I_v(x) e^{-x}$ is a monotonic decreasing function over $0 \leq x < \infty,\ v \geq -\frac{1}{2}$ [44], we write

$$I_{\frac{n}{2}-1}\left(\frac{2S\left(z+u\right)}{\sqrt{1+\Lambda}}\right) \leq \left(\frac{z+u}{z}\right)^{\frac{n}{2}-1} I_{\frac{n}{2}-1}\left(\frac{2Sz}{\sqrt{1+\Lambda}}\right) \exp\left(\frac{2Su}{\sqrt{1+\Lambda}}\right). \tag{5.14}$$

Applying (5.14) to G_3, we obtain an upper bound for G_3 as

$$G_3 \leq 2\exp\left(\frac{2Su}{\sqrt{1+\Lambda}}\right) \int_0^\infty \frac{(z+u)^{n-1}}{z^{\frac{n}{2}-1}} e^{-z^2} I_{\frac{n}{2}-1}\left(\frac{2Sz}{\sqrt{1+\Lambda}}\right) dz. \tag{5.15}$$

We note that since $n \in \mathbb{N}$, we can expand $(z+u)^{n-1}$ using the binomial theorem, obtaining an integral solvable in closed form with the integral identity [40, Eq. (6.643.2)] and [40, Eq. (9.220.2)], resulting in

$$\begin{aligned} G_3 \leq & \left(\frac{S}{\sqrt{1+\Lambda}}\right)^{\frac{n}{2}-1} \exp\left(\frac{2Su}{\sqrt{1+\Lambda}} + \frac{S^2}{1+\Lambda}\right) \\ & \times \sum_{i=0}^{n-1} \binom{n-1}{i} u^i {}_1F_1\left(\frac{i}{2}; \frac{n}{2}; -\frac{S^2}{1+\Lambda}\right). \end{aligned} \tag{5.16}$$

The results in (5.13) and (5.16) allow us to find an upper bound on G_1 as

$$G_1 \leq \frac{1}{(1+\Lambda)^{\frac{n}{2}}} \exp\left(u^2 + \frac{2Su}{\sqrt{1+\Lambda}} - \frac{\Lambda S^2}{1+\Lambda}\right)\left[\sum_{i=0}^{n} a_i u^i\right] \tag{5.17}$$

$$a_i = \begin{cases} \binom{n-1}{i}{}_1F_1\left(\frac{i}{2}; \frac{n}{2}; -\frac{S^2}{1+\Lambda}\right) & i = 0, \ldots, n-1 \\ \frac{2}{\Gamma\left(\frac{n}{2}\right)} \exp\left(\frac{-S^2}{1+\Lambda}\right) & i = n \end{cases}. \tag{5.18}$$

Although we have found an upper bound for G_1 which is in the desired closed form, we cannot partition (5.17) into a product of L independent functions. Since u^i for $i \in \mathbb{N}, u \geq 0$ is a convex function we can obtain, via Jensen's inequality, the following

$$\left(\sum_{k=1}^{L} \frac{r_k\sqrt{\sigma_k^2\lambda_k^2}}{2\sqrt{1+\Lambda\Omega_k^2}}\right)^i \leq \sum_{k=1}^{L} \frac{\lambda_k^2}{\Lambda\left(1-\lambda_k^2\right)}\left(\frac{\Lambda r_k}{\sqrt{\left(1+\Lambda\right)\sigma_k^2\lambda_k^2}}\right)^i. \tag{5.19}$$

Eq. (5.19), when combined with the inequality $1 + \sum_{k=1}^{N} b_k \leq \prod_{k=1}^{N}(1 + b_k)$, $b_k \geq 0$, allows us to find a suitable upper bound for G_1 as

$$\begin{aligned} G_1 \leq \frac{\exp\left(-\frac{\Lambda}{\Lambda+1}S^2\right)}{(1+\Lambda)^{\frac{n}{2}}} \prod_{k=1}^{L} \exp\left(\frac{\Lambda}{1+\Lambda}\frac{r_k^2}{2\Omega_k^2} + \frac{S}{1+\Lambda}\frac{r_k\sqrt{\lambda_k^2\sigma_k^2}}{\Omega_k^2}\right) \\ \times \left[1 + \frac{\lambda_k^2}{\Lambda\left(1-\lambda_k^2\right)}\sum_{i=1}^{n} a_i\left(\frac{\Lambda r_k}{\sqrt{1+\Lambda}\sqrt{\sigma_k^2\lambda_k^2}}\right)^i\right]. \end{aligned} \tag{5.20}$$

Finally, by substituting (5.20) into (5.9) we obtain the upper bound of joint

PDF of the generalized Rician distribution as

$$
\begin{aligned}
&f_{\mathbf{R}}(r_1,\ldots,r_L)\\
&\quad\leq \frac{\exp\left(-\frac{\Lambda}{\Lambda+1}S^2\right)}{(1+\Lambda)^{\frac{n}{2}}\Gamma^L\left(\frac{n}{2}\right)}\prod_{k=1}^{L}\left[1+\frac{\lambda_k^2}{\Lambda\left(1-\lambda_k^2\right)}\sum_{i=1}^{n-1}a_i\left(\frac{\Lambda r_k\sqrt{1-\lambda_k^2}}{\sqrt{1+\Lambda}\sqrt{2\Omega_k^2\lambda_k^2}}\right)^i\right]\\
&\qquad\times\frac{2r_k^{n-1}}{2^{\frac{n}{2}}\Omega_k^n}\exp\left(-\frac{1}{1+\Lambda}\frac{r_k^2}{2\Omega_k^2}+\frac{S}{1+\Lambda}\frac{r_k\sqrt{\lambda_k^2\sigma_k^2}}{\Omega_k^2}\right). \qquad (5.21)
\end{aligned}
$$

As in the case with the lower bound of the joint PDF, by letting $\lambda_k = 0,\ k = 1,\ldots,L$, we can show the equality in (5.21) is obtained for the Nakagami-m fading with independent branches.

5.3 Error Bounds

In this section we use the lower and upper bounds on the joint PDF in (5.5) and (5.21) respectively, to bound the error rate of an EGC combiner. As in Chapter 3, we perform error analysis on the equivalent channel at the output of the combiner $h_{EGC} = \sqrt{\gamma_{EGC}} = \frac{1}{L}\sum_{k=1}^{L} R_k$.

An alternate equation for the average error probability can be found by applying Parseval's theorem to (3.2) [45]:

$$
P_e = \frac{1}{\pi}\int_0^{\infty}\Re\left\{G^*(\omega)\,\Phi_{h_{EGC}}(\omega)\right\}d\omega \qquad (5.22)
$$

where $\Phi_{h_{EGC}}(\omega)$ is the CHF of h_{EGC} and $G(\omega)$ is the Fourier transform of

the conditional error probability. A full list of $G(\omega)$ for various coherent and noncoherent modulations is given in [Table 1][45]. For example, $G(\omega)$ for BPSK is given by

$$G\left(\omega\right)=\frac{1}{2\omega}\left\{\frac{2}{\sqrt{\pi}}F\left(\frac{\omega}{2}\right)+j\left[1-\exp\left(-\frac{\omega^{2}}{4}\right)\right]\right\}. \tag{5.23}$$

It is apparent that using upper or lower bounds on $\Phi_{h_{EGC}}\left(\omega\right)$ in the integration of (5.22) results in upper or lower bounds on P_e as

$$P_e \geq P_{e,L}=\frac{1}{\pi}\int_{0}^{\infty}\Re\left\{G^{*}\left(\omega\right)\Phi_{h_{EGC},L}\left(\omega\right)\right\}d\omega \tag{5.24}$$

$$P_e \leq P_{e,H}=\frac{1}{\pi}\int_{0}^{\infty}\Re\left\{G^{*}\left(\omega\right)\Phi_{h_{EGC},H}\left(\omega\right)\right\}d\omega \tag{5.25}$$

where $\Phi_{h_{EGC},L}\left(\omega\right)$ and $\Phi_{h_{EGC},H}\left(\omega\right)$ are the upper and lower bounds respectively on $\Phi_{h_{EGC}}(\omega)$ found using (5.5) and (5.21). From the definition of the CHF we have

$$\Phi_{h_{EGC}}(\omega)=\underbrace{\int_{0}^{\infty}\cdots\int_{0}^{\infty}}_{L}e^{j\frac{\omega}{\sqrt{L}}\sum_{k=1}^{L}r_k}f_{\mathbf{R}}(r_1,r_2,\ldots,r_L)dr_1dr_2\cdots r_L. \tag{5.26}$$

In both cases, substituting (5.5) or (5.21) into (5.26) to find $\Phi_{h_{EGC},L}\left(\omega\right)$ or

$\Phi_{h_{EGC},H}(\omega)$, respectively requires integral identity

$$\int_0^\infty \frac{x^{n+i-1}}{\alpha^{n+i}\Gamma(n)} \exp\left(-\frac{x^2}{2\alpha^2}+\beta x\right) dx = (n)_i \, \tilde{D}_{-n-i}(-\alpha\beta) \tag{5.27}$$

which can be found from [40, Eq. (3.462.1)]. Here in (5.27), $\tilde{D}_{-n}(z)$ is the normalized parabolic cylinder function[2] and can be expressed in terms of the confluent hypergeometric function using [40, Eq. (9.240)]

$$\tilde{D}_{-n}(z) = \frac{1}{2^{\frac{n}{2}}}\left[\frac{\sqrt{\pi}}{\Gamma\left(\frac{n+1}{2}\right)} {}_1F_1\left(\frac{n}{2};\frac{1}{2};\frac{z^2}{2}\right) - \frac{\sqrt{2\pi}z}{\Gamma\left(\frac{n}{2}\right)} {}_1F_1\left(\frac{n+1}{2};\frac{3}{2};\frac{z^2}{2}\right)\right]. \tag{5.28}$$

From (5.5) we obtain the lower bound of the characteristic function

$$\Phi_{h_{EGC},L}(\omega) = \frac{\exp\left(-\frac{\Lambda}{\Lambda+1}S^2\right)}{(1+\Lambda)^{\frac{n}{2}}} \left(\frac{\Gamma\left(\frac{n+1}{2}\right)2^{\frac{n}{2}}}{\sqrt{\pi}}\right)^L \prod_{k=1}^{L} \tilde{D}_{-n}\left(\frac{-j\omega\Omega_k}{\sqrt{L}}\right) \tag{5.29}$$

and from (5.21), we obtain the upper bound of the characteristic function

$$\begin{aligned}\Phi_{h_{EGC},H}(\omega) = \frac{\exp\left(-\frac{\Lambda}{\Lambda+1}S^2\right)}{(1+\Lambda)^{(1-L)\frac{n}{2}}} \left(\frac{2^{\frac{n}{2}}\Gamma\left(\frac{n+1}{2}\right)}{\sqrt{\pi}}\right)^L \prod_{k=1}^{L}\Bigg[\tilde{D}_{-n}(-\beta_k) \\ + \frac{\lambda_k^2}{\Lambda(1-\lambda_k^2)} \sum_{i=1}^{n} \left(\frac{\Lambda\sqrt{1-\lambda_k^2}}{\sqrt{\lambda_k^2}}\right)^i \frac{a_i\,(n)_i}{2^{\frac{i}{2}}} \tilde{D}_{-n-i}(-\beta_k)\Bigg]\end{aligned} \tag{5.30}$$

where $\beta_k = \frac{S}{\sqrt{1+\Lambda}}\sqrt{\frac{2\lambda_k^2}{1-\lambda_k^2}} + j\omega\Omega_k\sqrt{\frac{1+\Lambda}{L}}$. We have made use of the Gauss duplication formula [40, Eq. (8.335.1)] in the derivation of (5.29) and (5.30).

[2] $\tilde{D}_p(z)$ is related to the parabolic cylinder function, $D_p(z)$, in [40] by $\tilde{D}_p(z) = e^{-\frac{z^2}{4}} D_p(z)$. We have elected to use this alternate notation for simplicity.

Both error bounds, (5.24) and (5.25), consist of a single integral of closed form functions with implementations in popular mathematical software. Therefore, they are similar in computational complexity to the exact analysis for independent branches found in [45] and far simpler than the exact results in [22] and [46] which use the generalized correlation model with $\lambda_k = \lambda,\ k = 1, 2 \ldots, L$, i.e. equally correlated branches.

5.4 Numerical Results

The upper and lower bounds we have developed, in addition to being asymptotically tight for correlated fading, are exact for independent fading. Thus we expect the bounds to be tighter for weaker correlation among branches. We can see this is indeed the case by comparing Fig. 5.1 and Fig. 5.2 which plot $P_{e,L}$ and $P_{e,H}$ along with the asymptotic results found in Chapter 3 for Rayleigh fading channels with coherent BPSK and equal average branch SNRs. The numerical results in Fig. 5.1 and Fig. 5.2 have power correlation matrices, where the (k, i)th element is given by (5.1), of

$$\mathbf{P}_1 = \begin{pmatrix} 1 & 0.518 & 0.656 \\ 0.518 & 1 & 0.518 \\ 0.656 & 0.518 & 1 \end{pmatrix} \tag{5.31}$$

and

$$\mathbf{P}_2 = \begin{pmatrix} 1 & 2.25 \times 10^{-2} & 2.03 \times 10^{-1} \\ 2.25 \times 10^{-2} & 1 & 7.29 \times 10^{-2} \\ 2.03 \times 10^{-1} & 7.29 \times 10^{-2} & 1 \end{pmatrix} \tag{5.32}$$

respectively. We observe that while both bounds approach simulation results asymptotically, the lower bound is a much tighter fit especially at the higher correlation of $\mathbf{P}_2$ in Fig. 5.1.

Additional scenarios with Nakagami-m and Rician fading channels are shown in Fig. 5.3 and Fig. 5.4 with power correlation matrices

$$\mathbf{P}_3 = \begin{pmatrix} 1 & 3.5 \times 10^{-3} & 1 \times 10^{-2} \\ 3.5 \times 10^{-3} & 1 & 2.25 \times 10^{-2} \\ 1 \times 10^{-2} & 2.25 \times 10^{-2} & 1 \end{pmatrix} \tag{5.33}$$

and

$$\mathbf{P}_4 = \begin{pmatrix} 1 & 0.174 & 0.237 \\ 0.174 & 1 & 0.138 \\ 0.237 & 0.138 & 1 \end{pmatrix} \tag{5.34}$$

respectively.

We can see in Figs. 5.1-5.4, that while both bounds approach simulation results asymptotically, the lower bound is a much tighter fit especially at higher correlation. This is to be expected given the extra inequalities needed to produce a suitable upper bound. In situations were the SER-SNR curve is concave, as is the case in Figs. 5.1-5.4, the asymptotic error rate approx-

imation underestimates the actual error rate at low SNR. Thus, we only require $P_{e,L}$ to determine the validity of the asymptotic approximation. Using just $P_{e,L}$, the asymptotic approximation approaches the exact error rate at around 24 dB and 20 dB for the Rayleigh fading scenarios in Fig. 5.1 and Fig. 5.2 respectively, at 22 dB for both the Nakagami-1.5 fading in Fig. 5.3 and Rician fading in Fig. 5.4. However, the SER-SNR curve is not always concave, as is the case for Rician fading with larger Rice factors as is shown in Fig. 3.3 in Chapter 3. In such cases, we will require $P_{e,H}$ to determine at what SNR the asymptotic error rate adequately approximates the exact error rate.

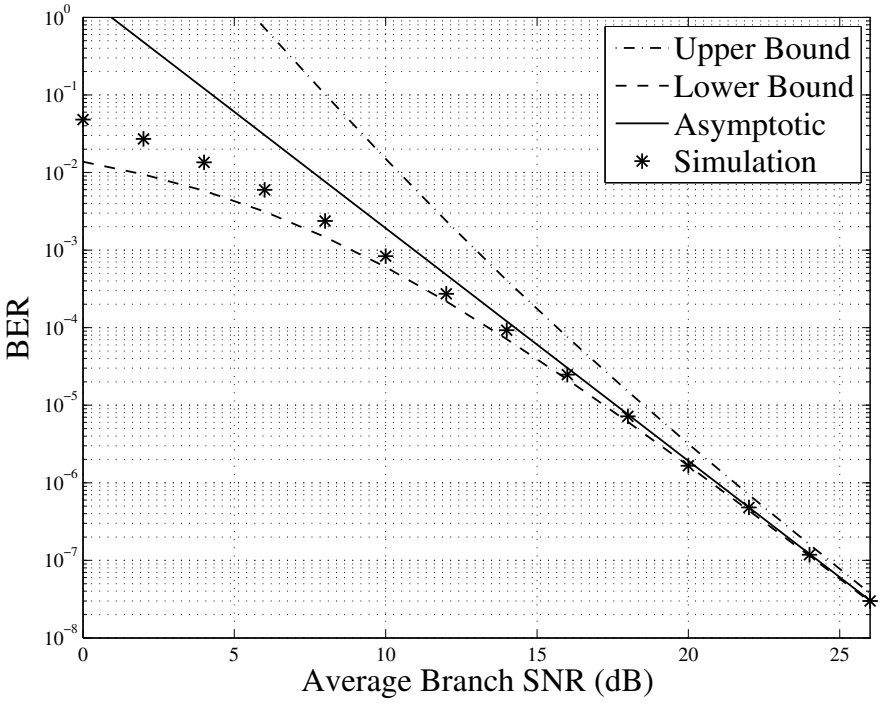

Figure 5.1: Upper and lower BER bounds of coherent BPSK over Rayleigh fading channels with triple branch EGC and equal average branch SNR. $\lambda = [0.9, 0.8, 0.9]$ and power correlation matrix $\mathbf{P}_1$.

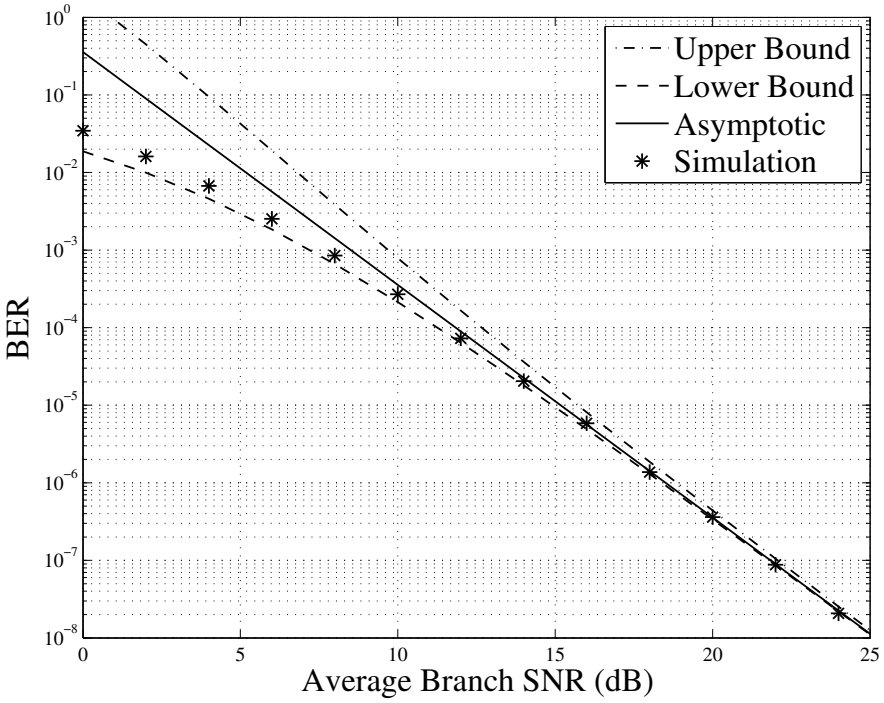

Figure 5.2: Upper and lower BER bounds of coherent BPSK over Rayleigh fading channels with triple branch EGC and equal average branch SNR. $\lambda = [0.5, 0.3, 0.8]$ and power correlation matrix $\mathbf{P}_2$.

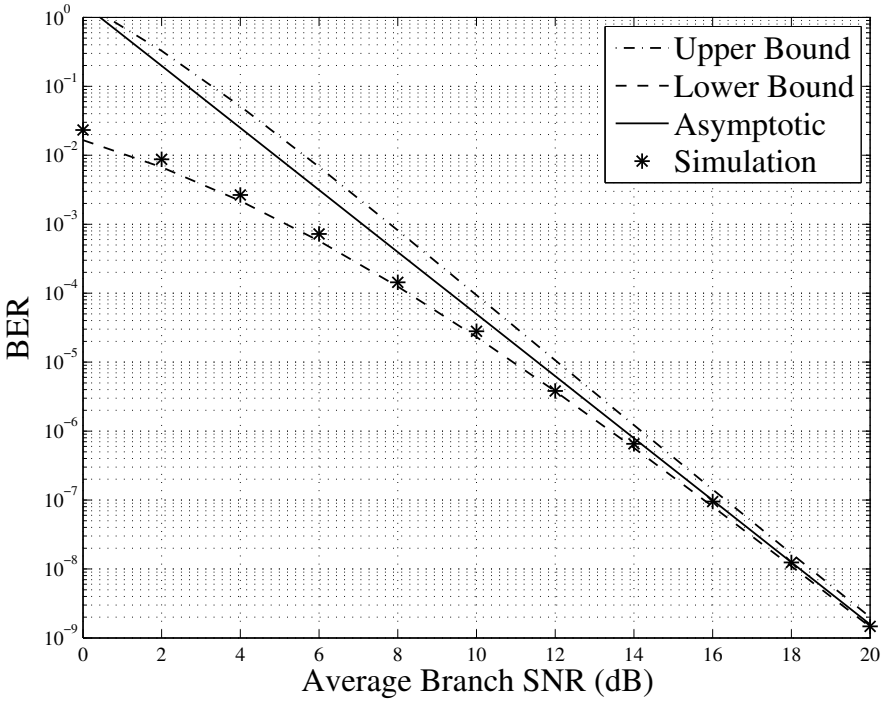

Figure 5.3: Upper and lower BER bounds of coherent BPSK over Nakagami-1.5 fading channels with triple branch EGC and equal average branch SNR. $\lambda = [0.2, 0.3, 0.5]$ and power correlation matrix $\mathbf{P}_3$.

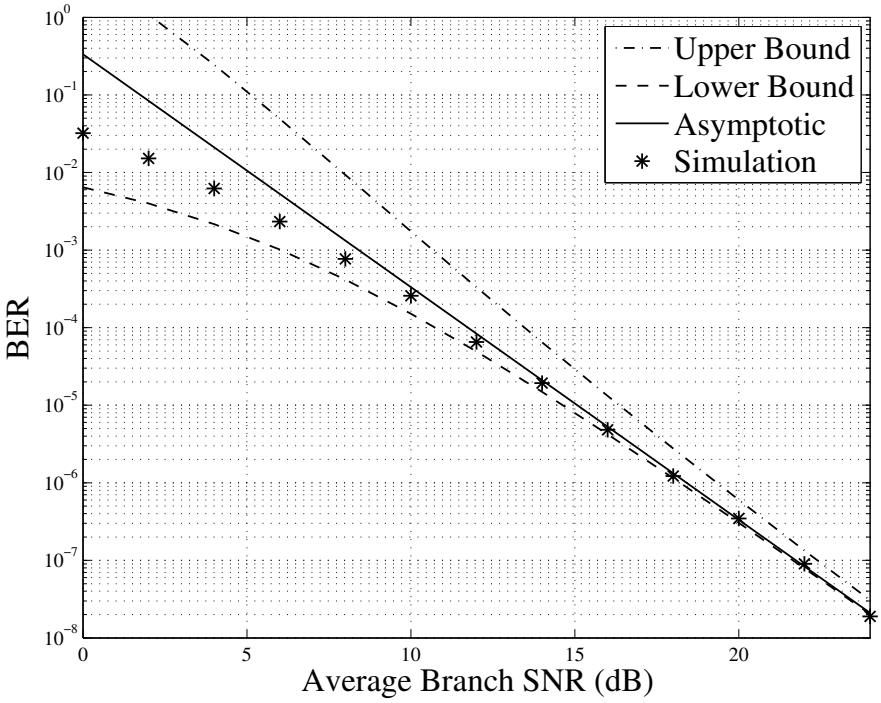

Figure 5.4: Upper and lower BER bounds of coherent BPSK over Rician fading channels ($S = 2$) with triple branch EGC and equal average branch SNR. $\lambda = [0.6, -0.4, 0.5]$ and power correlation matrix $\mathbf{P}_4$.

Chapter 6

Conclusion

6.1 Summary of Results

In this thesis we derived methods for improving and/or bounding the asymptotic error rates of SC and EGC over correlated generalized Rician fading channels. We first derived asymptotic error rates for SC, EGC, and MRC and compared their relative performance. The asymptotic results for SC were then extended into an exact infinite series for the SNR distributions and error rate for both coherent and noncoherent modulations. We proved that the series expansions for the SNR distributions converge unconditionally, and the error rate series expansion converges provided that the average SNR is sufficiently high. For all series, we provided truncation error bounds when the series is terminated at a finite number of terms. As the first term of the series expansions are the asymptotic results, this also provides an asymptotically tight bounds on the asymptotic results. Furthermore, we developed asymptotically tight bounds on the joint PDF of correlated generalized Rician RVs. Using this result, we then derived corresponding upper and lower bounds on the CHF of the root of the combined SNR and error rates for the EGC

combiner. The asymptotically tight bounds we have derived can be used to predict at what SNR value the asymptotic error rate can adequately approximate the exact error rate. This avoids time consuming multilevel numeric integration or Monte Carlo simulations that would otherwise be necessary. All our results have been verified by Monte Carlo simulations.

6.2 Future Work

The following is a list of possible future research opportunities:

- The Laguerre polynomial expansion of the Marcum Q-function could possibly be used to develop an infinite series expansion of the error rate of the EGC combiner.

- It may be feasible to extend the results for SC in Chapter 4 to the more general H-S/MRC. Using the joint PDF of generalized Rician RVs, the SNR MGF of an MRC can be found in closed form. With results for SC and MRC available, it is possible that similar results for H-S/MRC could be derived.

- Investigate other fading models. For example, single integral representations of the PDF and CDF of generalized correlated Weibull RVs are given in [24]. Thus, it is possible many of the ideas developed here could be applied to Weibull fading as well.

Bibliography

[1] M. K. Simon and M.-S. Alouini, *Digital Communications over Fading Channels*. New York: Wiley, 2000.

[2] V. Aalo, T. Piboongungon, and G. Efthymoglou, "Another look at the performance of MRC schemes in Nakagami-m fading channels with arbitrary parameters," *IEEE Transactions on Communications*, vol. 53, pp. 2002–2005, Dec. 2005.

[3] M.-S. Alouini, A. Abdi, and M. Kaveh, "Sum of gamma variates and performance of wireless communication systems over Nakagami-fading channels," *IEEE Transactions on Vehicular Communications*, vol. 50, pp. 1471–1480, Nov. 2001.

[4] V. Veeravalli, "On performance analysis for signaling on correlated fading channels," *IEEE Transactions on Communications*, vol. 49, pp. 1879–1883, Nov. 2001.

[5] M. Simon and M.-S. Alouini, "A unified performance analysis of digital communication with dual selective combining diversity over corre-

lated Rayleigh and Nakagami-m fading channels," *IEEE Transactions on Communications*, vol. 47, pp. 33–43, Jan. 1999.

[6] G. Vitetta, U. Mengali, and D. Taylor, "An error probability formula for noncoherent orthogonal binary FSK with dual diversity on correlated Rician channels," *IEEE Communications Letters*, vol. 3, pp. 43–45, Feb. 1999.

[7] R. Mallik, M. Win, and J. Winters, "Performance of dual-diversity predetection EGC in correlated Rayleigh fading with unequal branch SNRs," *IEEE Transactions on Communications*, vol. 50, pp. 1041–1044, Jul. 2002.

[8] C. Tellambura, A. Annamalai, and V. Bhargava, "Closed form and infinite series solutions for the MGF of a dual-diversity selection combiner output in bivariate Nakagami fading," *IEEE Transactions on Communications*, vol. 51, pp. 539–542, Apr. 2003.

[9] G. Karagiannidis, D. Zogas, and S. Kotsopoulos, "BER performance of dual predetection EGC in correlative Nakagami-m fading," *IEEE Transactions on Communications*, vol. 52, pp. 50–53, Jan. 2004.

[10] P. Bithas, G. Karagiannidis, N. Sagias, D. Zogas, and P. Mathiopoulos, "Dual-branch diversity receivers over correlated Rician fading channels," in *Proc. IEEE Vehicular Technology Conf. (VTC) 2005*, vol. 4, Dallas, Tx, Sept. 25-28 2005, pp. 2642–2646.

[11] G. Karagiannidis, D. Zogas, and S. Kotsopoulos, "Performance analysis of triple selection diversity over exponentially correlated Nakagami-m fading channels," *IEEE Transactions on Communications*, vol. 51, pp. 1245–1248, Aug. 2003.

[12] P. Dharmawansa, N. Rajatheva, and C. Tellambura, "Infinite series representations of the trivariate and quadrivariate Nakagami-m distributions," *IEEE Transactions on Wireless Communications*, vol. 6, pp. 4320–4328, Dec. 2007.

[13] G. Karagiannidis, D. Zogas, and S. Kotsopoulos, "On the multivariate Nakagami-m distribution with exponential correlation," *IEEE Transactions on Communications*, vol. 51, pp. 1240–1244, Aug. 2003.

[14] ——, "An efficient approach to multivariate Nakagami-m distribution using Green's matrix approximation," *IEEE Transactions on Wireless Communications*, vol. 2, pp. 883–889, Sep. 2003.

[15] Q. Zhang and H. Lu, "A general analytical approach to multi-branch selection combining over various spatially correlated fading channels," *IEEE Transactions on Communications*, vol. 50, pp. 1066–1073, Jul. 2002.

[16] R. de Souza and M. Yacoub, "On the mulitvariate $\alpha - \mu$ distribution with arbitrary correlation and fading parameters," in *Proc. IEEE Inter-*

national Conf. Communications (ICC) 2008, Beijing, China, May 19-23 2008, pp. 4456–4460.

[17] G. Karagiannidis, "Moments-based approach to the performance analysis of equal gain diversity in Nakagami-m fading," *IEEE Transactions on Communications*, vol. 52, pp. 685–690, May 2004.

[18] N. Zlatanov, Z. Hadzi-Velkov, and G. Karagiannidis, "An efficient approximation to the correlated Nakagami-m sums and its application in equal gain diversity receivers," *IEEE Transactions on Wireless Communications*, vol. 9, pp. 302–310, Jan. 2010.

[19] P. Sahu and A. Chaturvedi, "Performance analysis of predetection EGC in exponentially correlated Nakagami-m fading channel," *IEEE Transactions on Communications*, vol. 53, pp. 1252 – 1256, Aug. 2005.

[20] ——, "Performance analysis of a predetection EGC receiver in exponentially correlated Nakagami-m fading channels for noncoherent binary modulations," *IEEE Transactions on Wireless Communications*, vol. 5, pp. 1634–1638, Jul. 2006.

[21] Y. Chen and C. Tellambura, "Distribution functions of selection combiner output in equally correlated Rayleigh, Rician, and Nakagami-m fading channels," *IEEE Transactions on Communications*, vol. 52, pp. 1948–1956, Nov. 2004.

[22] ——, "Moment analysis of the equal gain combiner output in equally correlated fading channels," *IEEE Transactions on Vehicular Communications*, vol. 54, pp. 1971–1979, Nov. 2005.

[23] X. Zhang and N. Beaulieu, "Performance analysis of generalized selection combining in generalized correlated Nakagami-m fading," *IEEE Transactions on Communications*, vol. 54, pp. 2103–2112, Nov. 2006.

[24] N. Beaulieu and K. Hemachandra, "Novel simple representations for Gaussian class multivariate distributions with generalized correlation," *IEEE Transactions on Information Theory*, vol. 57, pp. 8072–8083, Dec. 2011.

[25] X. Li and J. Cheng, "Asymptotic error rate analysis of selection combining on generalized correlated Nakagami-m channels," *IEEE Transactions on Communications*, vol. 60, pp. 1765–1771, Jul. 2012.

[26] S. Liu, J. Cheng, and N. Beaulieu, "Asymptotic error rates of EGC and SC on Rician channels with arbitrary correlation," in *Proc. Canadian Workshop Information Theory*, Ottawa, Canada, May 13-15 2009, pp. 217–220.

[27] Z. Wang and G. Giannakis, "A simple and general parameterization quantifying performance in fading channels," *IEEE Transactions on Communications*, vol. 51, pp. 1389–1398, Aug. 2003.

[28] Y. Ma, "Impact of correlated diversity branches in Rician fading channels," in *Proc. IEEE International Conf. Communications (ICC) 2005*, vol. 1, Seoul, Korea, May 16-20 2005, pp. 473–477.

[29] A. F. Molisch, *Wireless Communications*, 2nd ed. New York: Wiley-IEEE Press, 2011.

[30] Y. Li and G. L. Stüber, *Orthogonal Frequency Division Multiplexing for Wireless Communications*. New York: Springer Publications, 2006.

[31] J. G. Proakis and M. Salehi, *Digital Communications*, 5th ed. New York: McGraw-Hill, 2008.

[32] M. Nakagami, "The m-distribution, a general formula of intensity distribution of rapid fading," in *Statistical Methods in Radio Wave Propagation*, W. G. Hoffman, Ed. Oxford, U.K.: Pergamon, 1960.

[33] H. Suzuki, "A statistical model for urban radio propogation," *IEEE Transactions on Communications*, vol. 25, pp. 673 – 680, Jul. 1977.

[34] W. Braun and U. Dersch, "A physical mobile radio channel model," *IEEE Transactions on Vehicular Technology*, vol. 40, pp. 472–482, May 1991.

[35] D. Brennan, "Linear diversity combining techniques," *Proc. IRE*, vol. 47, pp. 1075–1102, Jun. 1959.

[36] M.-S. Alouini and M. Simon, "Performance analysis of coherent equal gain combining over Nakagami-m fading channels," *IEEE Transactions on Vehicular Technology*, vol. 50, pp. 1449–1463, Nov. 2001.

[37] A. P. Prudnikov, Y. Brychkov, and O. Marichev, *Integrals and Series*. Gorden and Breach Science, 1998, vol. 4.

[38] A. Papoulis and S. U. Pillai, *Probability, Random Variables and Stochastic Processes*, 4th ed. New York: McGraw-Hill, 2002.

[39] M. Abramowitz and I. A. Stegun, Eds., *Handbook of Mathematical Functions with Formulas, Graphs, and Mathematical Tables*, 10th ed. New York: Dover Publications, 1972.

[40] I. S. Gradshteyn and I. M. Ryzhik, *Table of Integrals, Series, and Products*, 6th ed. San Diego: Academic Press, 2000.

[41] N. Beaulieu and A. Rabiei, "Linear diversity combining on Nakagami-0.5 fading channels," *IEEE Transactions on Communications*, vol. 59, pp. 2742–2752, Oct. 2011.

[42] S. András, Á. Baricz, and Y. Sun, "The generalized Marcum Q-function: an orthogonal polynomial approach," *Acta Universitatis Sapientiae Mathematica*, vol. 3, pp. 60–76, 2011.

[43] F. W. J. Olver, D. W. Lozier, R. F. Boisvert, and C. W. Clark, Eds., *NIST Handbook of Mathematical Functions*. New York, NY: Cambridge University Press, 2010.

[44] A. Baricz and Y. Sun, "New bounds for the generalized Marcum Q-function," *IEEE Transactions on Information Theory*, vol. 55, pp. 3091–3100, Jul. 2009.

[45] A. Annamalai, C. Tellambura, and V. Bhargava, "Equal-gain diversity receiver performance in wireless channels," *IEEE Transactions on Communications*, vol. 48, pp. 1732–1745, Oct. 2000.

[46] Y. Chen and C. Tellambura, "Performance of L-branch diversity combiners in equally correlated Rician fading channels," in *Proc. IEEE GLOBECOM 2004*, vol. 5, Dallas, Tx, Nov. 29-Dec. 3 2004, pp. 3379–3383.

Appendix A

Derivation of the Correlation Coefficient $\rho_{G_k G_i}$

The correlation coefficient by definition between G_k and G_i is

$$\rho_{G_k G_i} \triangleq \frac{\mathrm{E}\left[G_k G_i\right] - \mathrm{E}\left[G_k\right]\mathrm{E}\left[G_i\right]}{\sqrt{\mathrm{Var}[G_k]\mathrm{Var}[G_i]}}. \tag{A.1}$$

Since $G_k = \sum_{l=1}^{n} X_{kl}^2$, the term in numerator can be written as

$$\mathrm{E}\left[G_k G_i\right] - \mathrm{E}\left[G_k\right]\mathrm{E}\left[G_i\right] = \sum_{l=1}^{n}\sum_{j=1}^{n} \mathrm{E}\left[X_{kl}^2 X_{ij}\right] - \mathrm{E}\left[X_{kl}^2\right]\mathrm{E}\left[X_{ij}^2\right] \tag{A.2}$$

$$= \sum_{l=1}^{n} \mathrm{E}\left[X_{kl}^2 X_{il}^2\right] - \mathrm{E}\left[X_{kl}^2\right]\mathrm{E}\left[X_{il}^2\right] \tag{A.3}$$

where we have used the fact that X_{kl}^2 and X_{ij}^2 are independent for $l \neq j$. By examining (2.17) we note that X_{kl} and X_{il} consist of a component which is independent for $k \neq i$, i.e. U_{kl}, and a common component, U_{0l}. After substitution of (2.17) into (A.3) the independent components will cancel out

and the cross terms are zero since $\mathrm{E}\left[U_{kl}\right] = 0$ for $k \geq 1$, we are left with

$$\mathrm{E}\left[G_k G_i\right] - \mathrm{E}\left[G_k\right]\mathrm{E}\left[G_i\right] = \sigma_k^2\sigma_i^2\lambda_k^2\lambda_i^2 \sum_{l=1}^{n} \mathrm{E}\left[U_{0,l}^4\right] - \mathrm{E}\left[U_{0,l}^2\right]^2 \tag{A.4}$$

$$= \sigma_k^2\sigma_i^2\lambda_k^2\lambda_i^2\left(\frac{n}{2} + 2S^2\right) \tag{A.5}$$

where $S^2 = \sum_{l=1}^{n} m_l^2$. Since G_k is noncentral χ^2 distributed its variance is

$$\mathrm{Var}[G_k] = \sigma_k^4\left(\frac{n}{2} + 2\lambda_k^2 S^2\right). \tag{A.6}$$

Upon substituting (A.5) and (A.6) into (A.1) we obtain

$$\rho_{G_k G_i} = \frac{\lambda_k^2\lambda_i^2(\frac{n}{2} + 2S^2)}{\sqrt{\frac{n}{2} + 2\lambda_k^2 S^2}\sqrt{\frac{n}{2} + 2\lambda_i^2 S^2}}, \quad k \neq i. \tag{A.7}$$

Appendix B

Derivation of the Integral Identity (4.7)

Define

$$I = \int_0^\infty t^{i+\frac{\mu-1}{2}} e^{-\alpha t} I_{\mu-1}\left(2\beta\sqrt{t}\right) dt \tag{B.1}$$

where $i \in \mathbb{N}$ and $\mu > 0$, then from the integral identity [40, Eq. (6.643.2)] and [39, Eq. (13.1.32)] we have

$$I = (\mu)_i \left(\frac{\beta}{\alpha^i}\right)^\mu {}_1F_1\left(\mu + i; \mu; \frac{\beta^2}{\alpha}\right). \tag{B.2}$$

Using Kummer's transform ${}_1F_1(a;b;z) = e^z {}_1F_1(b-a;b;-z)$ [39], (B.2) becomes

$$I = (\mu)_i \left(\frac{\beta}{\alpha^i}\right)^\mu \exp\left(\frac{\beta^2}{\alpha}\right) {}_1F_1\left(-i; \mu; -\frac{\beta^2}{\alpha}\right). \tag{B.3}$$

Since i is a nonnegative integer, ${}_1F_1\left(-i;\mu;-\frac{\beta^2}{\alpha}\right)$ reduces to a generalized Laguerre polynomial [39, Eq. (13.6.9)] and we have

$$I = i! \left(\frac{\beta}{\alpha^i}\right)^\mu \exp\left(\frac{\beta^2}{\alpha}\right) L_i^{(\mu-1)}\left(-\frac{\beta^2}{\alpha}\right). \tag{B.4}$$